

JGR Solid Earth

RESEARCH ARTICLE

10.1029/2023JB028538

Key Points:

- Remagnetized Neoproterozoic carbonates in Brazil may not consistently display anomalous hysteresis parameters
- Synchrotron-based analysis revealed pseudo-single domain-sized magnetite spatially correlated with aluminosilicates (smectite-illite)
- The Late Cambrian assembly of Gondwana thermally reset the carbonates' remanence, eventually blocking it (470–460 Ma) during gradual cooling

Supporting Information:

Supporting Information may be found in the online version of this article.

Correspondence to:

U. D. Bellon and W. Williams,
ualisson.bellon@usp.br;
wyn.williams@ed.ac.uk

Citation:

Bellon, U. D., Trindade, R. I. F., Williams, W., Galante, D., Sant'Anna, L. G., & Pescarini, T. (2024). Clay minerals and continental-scale remagnetization: A case study of South American Neoproterozoic carbonates. *Journal of Geophysical Research: Solid Earth*, 129, e2023JB028538. <https://doi.org/10.1029/2023JB028538>

Received 20 DEC 2023

Accepted 22 SEP 2024

Author Contributions:

Conceptualization: Ualisson Donardelli Bellon, Ricardo Ivan Ferreira Trindade, Wyn Williams

Data curation: Ualisson Donardelli Bellon, Ricardo Ivan Ferreira Trindade, Wyn Williams, Douglas Galante, Lucy Gomes Sant'Anna, Thales Pescarini





Formal analysis: Ualisson Donardelli Bellon, Douglas Galante, Lucy Gomes Sant'Anna, Thales Pescarini

Funding acquisition: Ricardo Ivan Ferreira Trindade, Wyn Williams

© 2024. The Author(s).

This is an open access article under the terms of the [Creative Commons Attribution License](#), which permits use, distribution and reproduction in any medium, provided the original work is properly cited.

Clay Minerals and Continental-Scale Remagnetization: A Case Study of South American Neoproterozoic Carbonates

Ualisson Donardelli Bellon^{1,2} , Ricardo Ivan Ferreira Trindade¹ , Wyn Williams² , Douglas Galante³, Lucy Gomes Sant'Anna⁴, and Thales Pescarini¹ 

¹Department of Geophysics, University of São Paulo, Institute of Astronomy, Geophysics and Atmospheric Sciences (IAG), São Paulo, Brazil, ²School of Geosciences, University of Edinburgh, Edinburgh, Scotland, ³Department of Sedimentary and Environmental Geology, University of São Paulo, Institute of Geosciences, São Paulo, Brazil, ⁴Institute of Energy and Environment (IEE), São Paulo, Brazil

Abstract The Neoproterozoic carbonate rocks of the Araras Group (Amazon Craton) and the Sete-Lagoas and Salitre Formations (São Francisco Craton) share a statistically indistinguishable single-polarity (reversed) characteristic direction. This direction is associated with paleomagnetic poles that do not align with the expected directions for primary detrital remanence. We employ a combination of classical rock magnetic properties and micro imaging/chemical analysis (in thin sections) using synchrotron radiation to examine these remagnetized carbonate rocks. Magnetic data indicate that most samples lack the anomalous hysteresis properties typically associated with carbonate remagnetization (except for distorted loops). Through a combination of Scanning Electron Microscopy with Energy Dispersive X-ray Spectroscopy (SEM-EDS), X-ray Fluorescence (XRF), and X-ray Absorption Spectroscopy (XAS), we identified subhedral/anedral magnetite, or spherical grains with a core-shell structure of magnetite surrounded by maghemite. These grains are within the pseudo-single domain size range, as do most of the iron sulfides, and are spatially associated with potassium-bearing aluminosilicates. While fluid percolation and organic matter maturation play a role, smectite-illitization appears to be crucial for the growth of these phases. X-ray diffraction analysis, in addition, identifies these silicates as predominantly highly crystalline illite, suggesting exposure to epizone temperatures. These temperatures were likely reached during the final stages of the Gondwana assembly (Cambrian), but remanence was only locked in afterward, in successive cooling events during the Early Middle Ordovician. This is supported by the carbonates' paleomagnetic pole positions compared to Gondwana's apparent polar wander path, and the absence of reversals, contrasting with the high reversal frequency of the Late Ediacaran/Cambrian.

Plain Language Summary Carbonate rocks serve as important records of ancient climates and host magnetic minerals capable of documenting the evolution of Earth's magnetic field. Nevertheless, their original magnetization, acquired during sedimentation, is frequently supplanted by a secondary magnetization, originating from various geological processes altering local thermochemical stability. For carbonate rocks, this remagnetization process is often associated with a “magnetic fingerprint.” In South America, carbonate rocks from different sedimentary basins (hundreds of kilometers apart) exhibit statistically similar magnetic components that deviate from their formation origin, indicating secondary processes. This multidisciplinary study integrates classical paleomagnetic analysis with micro-chemical and imaging analysis to comprehend the geological phenomena responsible for remagnetizing such an extensive continental area. We demonstrate that not all remagnetized samples display the anticipated magnetic fingerprint. Highly detailed chemical analysis confirms the presence of nanoscopic magnetic minerals spatially correlated with clay minerals indicating that while organic matter transformation may play a significant role, clay mineral transformation is a key phenomenon governing remagnetization in these rocks. However, our data also supports the notion that these rocks underwent heating during the final assembly of the ancient continental landmass, Gondwana, and a sequential cooling event is suggested as locking their magnetization in the state observed today.

1. Introduction

Carbonate sedimentation, often marine-derived (Grotzinger & James, 2000), correlates paleomagnetic data with significant geological and evolutionary events (Golovanova et al., 2023; Trindade et al., 2003; Trindade & Macouin, 2007). However, challenges arise in identifying primary detrital remanence due to single-polarity components that mismatch the rock's geochronological age (Elmore et al., 2012), likely altered by geological

Investigation: Ualisson Donardelli Bellon, Douglas Galante
Methodology: Ualisson Donardelli Bellon
Project administration: Ricardo Ivan Ferreira Trindade, Wyn Williams
Resources: Ricardo Ivan Ferreira Trindade
Supervision: Ricardo Ivan Ferreira Trindade, Wyn Williams
Validation: Ualisson Donardelli Bellon
Visualization: Ualisson Donardelli Bellon
Writing – original draft: Ualisson Donardelli Bellon
Writing – review & editing: Ricardo Ivan Ferreira Trindade, Wyn Williams, Douglas Galante, Lucy Gomes Sant’Anna, Thales Pescarini

processes below the Curie temperature (Jackson & Swanson-Hysell, 2012), leading to secondary remanence or remagnetization.

Remagnetization can occur through thermal or chemical phenomena. Thermal effects partially or completely overwrite remanence by achieving the relaxation time of grain populations at specific temperatures. Chemically, transformations below the Curie temperature may develop a chemical remanent magnetization (CRM) (Dunlop & Özdemir, 1997; Levi, 2007), which includes grain growth remanent magnetization (g-CRM) and alteration chemical remanence (a-CRM) (Tauxe et al., 2018). The chemical stability of the magnetic mineralogy is controlled by the redox state (Pourbaix, 1974) and the chemical composition of seawater and pore water. The authigenic particles formed in this process, when transitioning from superparamagnetic (SP) to single-domain (SD) states, will become stable geomagnetic recorders (Dunlop & Özdemir, 1997).

Carbonate rocks are exemplary for studying CRMs due to distinct magnetic properties or “magnetic fingerprints” of remagnetization, as globally observed (Elmore et al., 2012; Jackson, 1990; Jackson & Swanson-Hysell, 2012). These include abnormal amounts of superparamagnetic (SP) grains; anomalous hysteresis ratios, followed by distorted loops (e.g., wasp-waists and potbellies); and contradictory domain tests. Chemical remagnetization may occur through sediment burial and fluid migration. Early diagenetic processes during sediment burial are influenced by redox conditions and microbial respiration, which may utilize iron oxides/hydroxides along with organic matter, reducing ferric ions (Roberts, 2015). Late diagenetic processes, such as clay-mineral transformations, release ions (including ferrous ions) conducive to authigenic ferromagnetic phase growth (Hirt et al., 1993; Tohver et al., 2008; Woods et al., 2002). Fluid transport through sedimentary rock porosity can induce mineral transformations, while nearby magmatic activity or orogenies, involving hot basinal brines and hydrothermal processes, may dissolve detrital phases and foster new growths (D’Agrella-Filho et al., 2000; Dannemann et al., 2022; Davidson et al., 2000; Huang et al., 2017; Jackson, 1990; Jiao et al., 2019; McCabe & Elmore, 1989; McCabe et al., 1983; Miller & Kent, 1988; Oliver, 1986; Stamatakis et al., 1996; Trindade et al., 2004; Xu et al., 2022). Additionally, organic matter maturation and hydrocarbon biodegradation in sedimentary basins may produce redox variations that disturb the local thermochemical equilibrium, further contributing to new magnetic phase formation (Aldana et al., 2011; Emmerton et al., 2013; Font et al., 2006).

Despite identifying various processes linked to remagnetization, establishing connections on a continental scale remains challenging. Neoproterozoic carbonates across South America present a unique puzzle, with reports of widespread remagnetization processes in the Río de la Plata (Rapalini & Bettucci, 2008; Rapalini et al., 2013), Amazon (Trindade et al., 2003), and São Francisco (D’Agrella-Filho et al., 2000) Cratons. Here, we focus on the cap carbonates of this age found within Brazilian territory (Amazon and São Francisco Cratons). These carbonates display an almost indistinguishable single-polarity (reversed) characteristic direction (D’Agrella-Filho et al., 2000; Font et al., 2005, 2006, 2012; Trindade et al., 2003, 2004) despite vast geographic separations and diverse cratonic regions (see Figures 1a and 1b). This study employs a multidisciplinary approach, combining bulk macroscopic magnetic property measurements with synchrotron-based microscopic chemical and imaging analyses to explore spatial relationships of remanence-bearing grains with surrounding minerals, particularly clays. Additionally, we reassess magnetic signatures, questioning the reliability of traditional remagnetization “fingerprints,” as well as delve into the particular phenomena that might have led to the remagnetization of these rocks.

2. Geological Setting and Previous Studies

Remagnetized carbonates extend across Brazil, from the Amazon to the São Francisco-Congo Craton (Font et al., 2012). Our study targets three different basins shown in Figure 2: the cap carbonates of the Sete Lagoas Formation (Bambu Group, São Francisco Basin); the carbonates of the Salitre Formation (Irecê Basin) in the São Francisco Craton (Figure 2a); and the carbonates of the Araras group on the Amazon craton and the Paraguay belt, the bituminous limestones of the Guia Formation at Terconi and Cáceres (Figures 2b and 2e). The geological settings of these units and findings from previous studies are summarized in the following section.

2.1. The São Francisco and Irecê Basins

The Neoproterozoic São Francisco Basin is divided into the Macaúbas Group at its base and the Bambuí Group overlying it. The Bambuí Group contains a thick sequence of more than 1,000 km of siliciclastic and carbonate deposits and is segmented into two subgroups: a basal marine stratum with carbonate and pelitic-psammitic

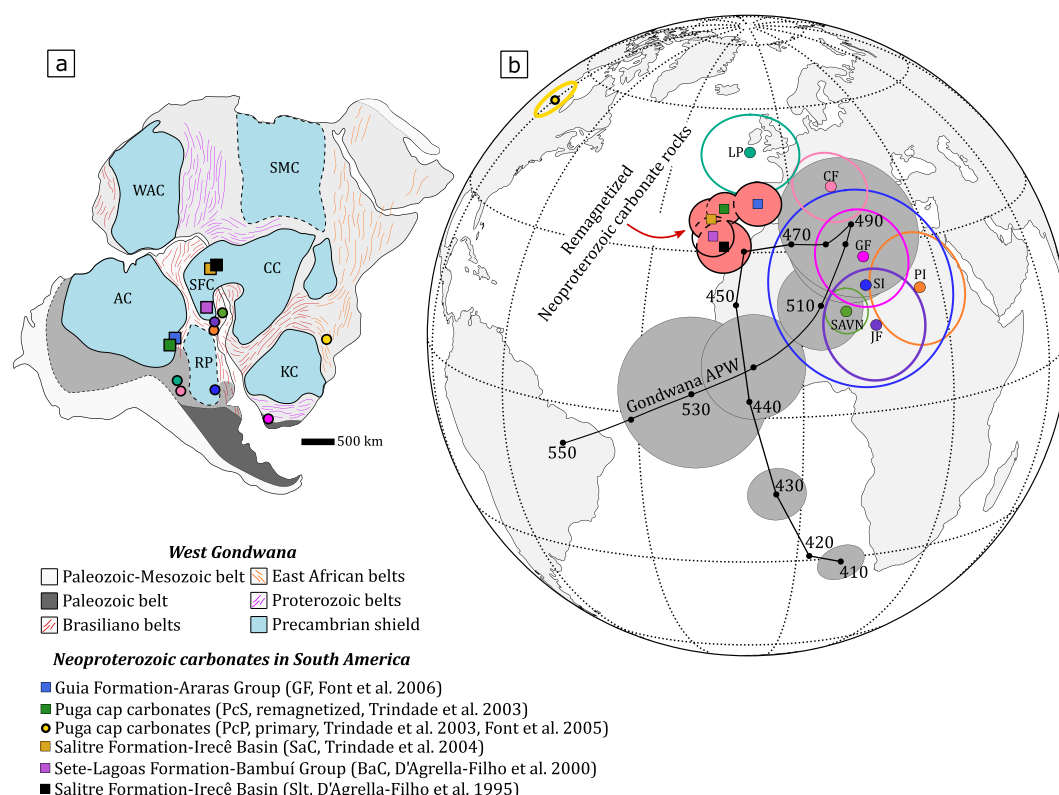


Figure 1. (a) Tectonic context of the geological targets studied in this project. Spheres and squares show the geographic location of the paleomagnetic poles from (b), modified from Alkmim et al. (2006). (b) APW curve of West Gondwana considering South Africa in its current position, from Torsvik et al. (2012), showing mean paleomagnetic poles of millions of years old ages ($A_{95} < 10^\circ$, gray circles). Poles represented by a sphere are Late Neoproterozoic/Early Cambrian and their respective A_{95} interval, rotated to South Africa (55.7° , -34.8° , 43.3°) when necessary. Squares are paleomagnetic poles of remagnetized carbonates, centered at their A_{95} interval (pinkish). Notice how the confidence intervals of Neoproterozoic remagnetized poles from South America intersect themselves. AC: Amazon craton, WAC: West-African craton, CC: Congo Craton, SFC: São Francisco craton, RP: Rio de la Plata craton, KC: Kalahari craton, SMC: Sahara Meta craton. Paleomagnetic poles of remagnetized carbonates are BaC, SaC, Sl, GF, and PcS; PcP refers to the primary remanence held by the carbonates at the base of Mirassol d'Oeste formation; other West-Gondwana Late Neoproterozoic/Early Cambrian poles are: SAVN, JF, PI, SI, CF, LP, and GF. See Table 1 for reference.

sediments, and an upper alluvial stratum. Deformation increases progressively toward the Brasília and Araçuaí orogens, with two central regions remaining undeformed (D'Agrella-Filho et al., 2000; Dardenne & Freitas-Silva, 1998).

Direct dating of cap carbonates at the base of the Sete Lagoas Formation provided an age of 740 ± 22 million years (Ma) (Babinski et al., 2007). The paleomagnetic analysis identified three magnetic components: an unstable northwest (NW) component A, a more stable northeast (NE) component B, and component C, which closely resembles B but with higher blocking temperatures (D'Agrella-Filho et al., 2000). While B and C components represent ancient geomagnetic signals unrelated to depositional remanence, A is interpreted as a later viscous component. Moreover, anomalous hysteresis ratios and other characteristics suggest the rocks are remagnetized carbonates.

The Bebedouro and Salitre formations in the Irecê Basin are analogous to the Macaúbas and Bambuí Groups. The Bebedouro Formation contains glacial and marine deposits, with detrital zircons dating to around 875 Ma (Babinski et al., 2004; Figueiredo et al., 2009). The Salitre Formation, a marine platform carbonate deposit, features cap-carbonate characteristics like columnar stromatolites (Misi & Kyle, 1994). Isotopic dating using strontium ratios placed the age of the Salitre Formation at 600–670 Ma (Misi & Veizer, 1998), and recent studies reported a maximum depositional age of around 670 Ma (Santana et al., 2021). Further studies of Trindade et al. (2004) identified a multicomponent paleomagnetic signature in the Salitre Formation similar to that of the

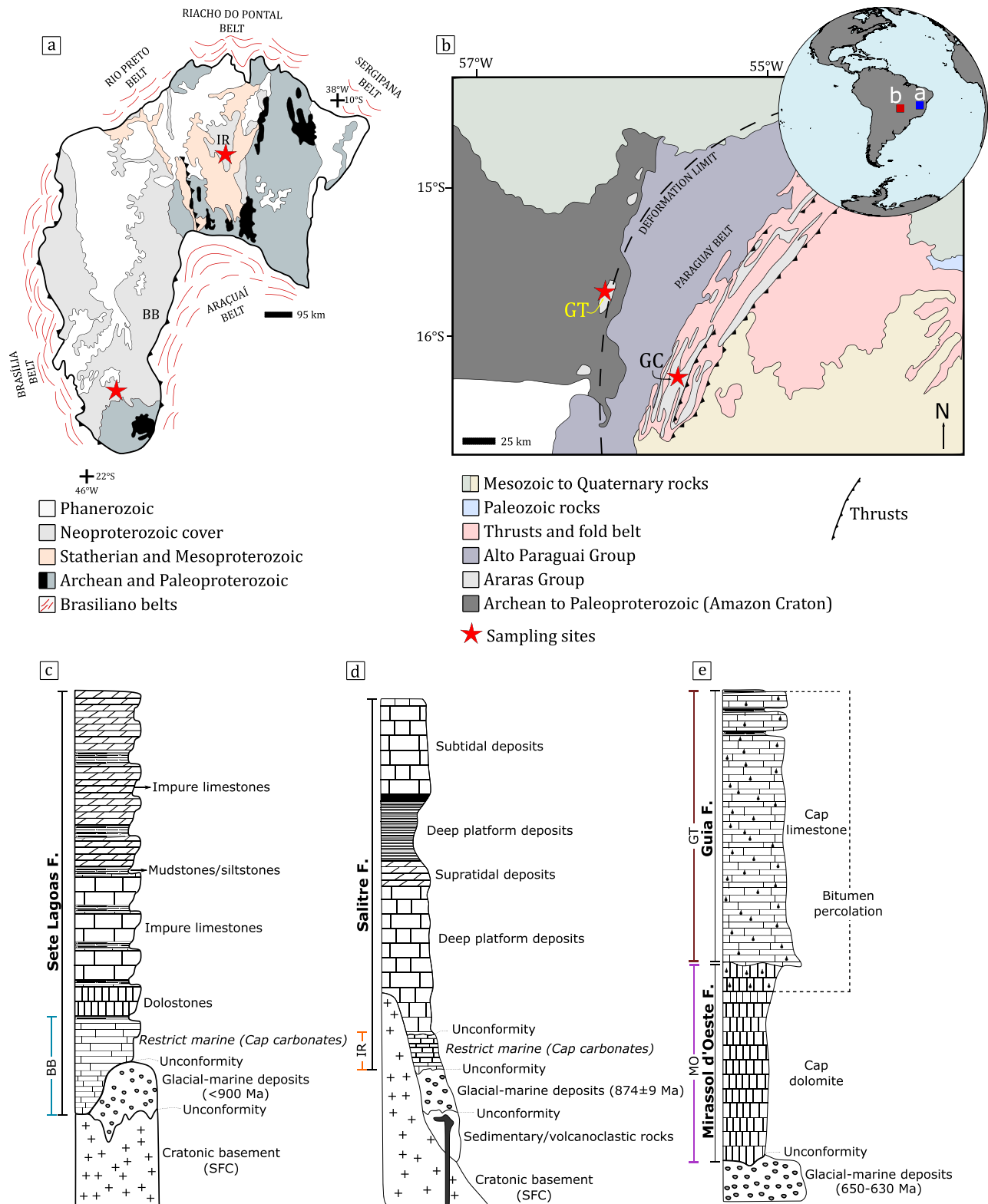


Figure 2.

Sete Lagoas Formation. Poles derived from each of the components match with those of the Bambuí (see Figure 1b). This suggests that remagnetization throughout the São Francisco craton resulted from a regional scale event, previously interpreted as a percolation of saline fluids around 520 Ma (D'Agrega-Filho et al., 2000; Trindade et al., 2004). These studies have pointed out that fluids likely triggered the crystallization of authigenic ferrimagnetic minerals, causing the magnetic remanence in components B and C (Table 1). While hypotheses exist regarding the mechanism behind this remagnetization, the process responsible for the growth of ferrimagnetic grains and the acquisition of secondary remanence remains uncertain.

2.2. The Araras Group

The Araras Group overlies the Puga Formation, a glaciomarine sequence of siltstones and diamictites (Alvarenga & Trompette, 1992). In this group, post-glacial cap carbonates are followed by lime mudstones and shales that represent deep platform deposits (Nogueira et al., 2003; Trindade et al., 2003). While radiometric dating for the Araras Group is unavailable, the overlying Alto Paraguay Group has an estimated age of 569 ± 20 Ma (Rb-Sr) (Riccomini et al., 2007), and a granite intrusion into correlated sedimentary rocks in the Paraguay belt (see Figure 2) provides a minimum age of 528 Ma (Guimarães et al., 2017). Besides, macrofossils from the Corumbá Group, which is stratigraphically linked to the Araras, hint at an Ediacaran biota (Gaucher et al., 2003; Nogueira & Riccomini, 2006).

At the base of the Araras Group is the Mirassol d'Oeste Formation, composed of laminated pinkish dolomitic mudstones and gray dolomites, which is overlaid by the Guia Formation, consisting of bituminous limestones with terrigenous grains (Font et al., 2006). The layers remain sub-horizontal and undisturbed over the Amazon Craton but are highly deformed in the Paraguay Belt (Figure 2b). In the Amazon Craton, the Araras Group is a compelling case for remagnetization studies, as part of its basal unit has preserved depositional remanence, while its upper unit is remagnetized. Paleomagnetic studies identified two components: Component A (dual polarity) in the Puga cap dolomite (base of the Mirassol d'Oeste, see the pole PcP in Table 1), with high unblocking temperatures around 680°C (Font et al., 2005); and Component B, whose poles align with the Irecê and Bambuí formations (Table 1), which Trindade et al. (2003) suggest as a Middle-to-Late Cambrian remagnetization (Figure 1b). Further research into the Mirassol d'Oeste Formation found a dual polarity remanence with high unblocking temperatures and a paleolatitude of 22°, indicating that a mixture of hematite and magnetite carries the remanence of both polarities (Font et al., 2005). However, Trindade et al. (2003) studies found magnetite to be the primary remanence mineral, which might imply local sedimentary heterogeneities.

The Guia Formation is more enriched in bitumen than the underlying Mirassol d'Oeste Formation. Its remanence was studied in two areas: the Tercony Quarry (Amazon Craton) and the Cáceres region (Paraguay Belt, Figure 1b). Thermal demagnetization revealed a single polarity component (Table 1) that also matches the other remagnetized Neoproterozoic carbonate rocks of South America (Font et al., 2006). Samples from the Paraguay Belt had more superparamagnetic particles than the Mirassol d'Oeste Formation. Hints of the remagnetization phenomenon in the Araras Group were described by Font et al. (2006), whereas over the underformed region hydrocarbon maturation was believed to support most of the authigenic generation of monoclinic pyrrhotite; while over the deformed region, the hydrocarbon maturation paired with smectite illitization, possibly triggered by tectonism, would eventually culminate in the generation of both pyrrhotite and magnetite (Font et al., 2006).

3. Methods

In pursuit of understanding the geological mechanisms responsible for remagnetizing widely separated basins, this research aims to conduct a detailed and multidisciplinary study. In our selection, if the measured magnetic properties of the selected samples align with the expected magnetic fingerprints of remagnetized carbonates, a comprehensive analysis was then employed from macro to micro scales. The methodology begins by

Figure 2. Simplified geological context of the studied units. (a) São Francisco Craton, showing the basins of Irecê (IR) and São Francisco, where the Bambuí Group lies (BB), surrounded by Neoproterozoic orogenies. Modified from Paula-Santos et al. (2015); (b) Tectonic map of the southeast part of the Amazon Craton and the Paraguay belt, showing the distribution of the Araras Group in both terranes. Modified from Font et al. (2006) after Nogueira et al. (2003); (c–e) are representative stratigraphic profiles of sections of the Bambuí Group, Irecê Basin, and Araras Group (over the Amazon Craton), modified from Guacaneme et al. (2017), Santana et al. (2021), and Trindade et al. (2003), respectively. Notice that the stratigraphic sectors where the samples come from are indicated in the profiles. GT stands for Guia formation (Tercony), and MO stands for Mirassol d'Oeste formation.

Table 1

Paleomagnetic Poles of Remagnetized Carbonates in the Amazon and São Francisco Cratons, in Comparison With Other Matching Paleomagnetic Poles of Similar Age (Same as in Figure 1)

Source	Age (Ma)	PLAT	PLON	A95	Reference
BaC (r)	500–530?	30.2°	321.0°	3.8°	D'Agrella-Filho et al. (2000)
SaC (r)	500–530?	33.0°	323.0°	4.0°	Trindade et al. (2004)
Slr (r)	≈500?	27.5°	321.4°	4.9°	D'Agrella-Filho (1995)
GF (r)	≈520?	29.9°	332.6°	4.3°	Font et al. (2006)
PcS (r)	≈520?	33.1°	326.6°	3.2°	Trindade et al. (2003)
PcP (p)	580–600?	83.5°	283.7°	4.5°	Trindade et al. (2003), Font et al. (2005)
SAVN (p)	500	4.7°	333.2°	4.06°	Temporim et al. (2021)
PI (r)	510–500	−0.8°	346.5°	10.2°	D'Agrella-Filho and Pacca (1986)
JF (r)	510–500	−0.6°	335.2°	10.0°	D'Agrella-Filho et al. (2004)
SI (p)	≈520	5.9°	338.1°	18.1°	Sánchez-Bettucci and Rapalini (2002)
CF (p)	≈519	23.6°	346.5°	7.0°	Franceschinis et al. (2019)
LP (p)	477–485	38.3°	340.4°	8.8°	Piceda et al. (2018)
GF (p)	≈485	28.0°	14.0°	9.0°	Bachtadse et al. (1987)

Note. (p)—Primary Magnetization; (r)—Remagnetization; (?)—indicates that age is uncertain.

characterizing the magnetic assemblages of samples collected from locations previously investigated in paleomagnetic studies (D'Agrella-Filho et al., 2000; Trindade et al., 2004; Font et al., 2006). When samples with the expected magnetic signatures of chemically remagnetized rocks were identified, compositional analysis was carried out.

Samples from the Guia Formation are designated by their specific locations: GC (Cáceres, Figure 2b) from the deformed terrain and GT (Terconi, Figures 2b and 2e) over the Amazon Craton. The basal Mirassol d'Oeste Formation (MO, also in the Terconi quarry, Figure 2e), primarily known for carrying only a primary magnetic component, is re-examined to check for any potential false-positive remagnetization signals. In the Irecê Basin, samples from the Salitre Formation are labeled IR (Figures 2a and 2d), while those from the Sete Lagoas Formation in the Bambuí Group are denoted as BB (Figures 2a and 2c). We have not conducted new fieldwork; instead, we have utilized samples previously collected in other works (D'Agrella-Filho et al., 2000; Trindade et al., 2004; Font et al., 2006). For clarification on the correspondence between our sample codes and the original sample names, please refer to the spreadsheet available in the repository where our data is stored (visit the URL at Bellon, Williams, et al. (2023)).

3.1. Rock Magnetism

The classical cylindrical paleomagnetic specimens, sampled during the original fieldwork campaigns by D'Agrella-Filho et al. (2000), Trindade et al. (2004), and Font et al. (2006), are the focus of our study. To characterize the remanence carriers, anhysteretic remanent magnetizations (ARMs) were induced in alternating field (AF)-demagnetized samples using a Long Core SQUID magnetometer (2G Enterprises), applying a direct current (DC) field of 100 μ T and AF fields ranging from 0 to 100 mT along the Z-axis.

Since grains in the SP and SD states may significantly influence the remagnetization fingerprints in carbonates (Jackson & Swanson-Hysell, 2012), we aimed to semi-quantify their presence by measuring the magnetic susceptibility (of the cylindrical specimens) at low and high frequencies, as well as the in-phase angle magnetic susceptibility using an Agico Kappabridge MFK1. Magnetic susceptibility was measured five times consecutively for each sample, and their arithmetic mean was calculated. These measurements were performed in a room with a controlled temperature of 21°C and completed on the same day to minimize instrumental disturbance.

Frequency-dependent magnetic susceptibility is traditionally used to identify grains within the SP and SD threshold (Hrouda et al., 2013). The standard frequencies are 976 Hz (low frequency) and 15,616 Hz (high frequency), which we used to measure susceptibility under a low-intensity AC field of 200 A m^{−1}. The parameter

χ_{FD} (Equation 1), introduced by Dearing et al. (1996), measures the percentage loss in susceptibility between low and high frequencies (related to ultrafine ferromagnetic particles) using χ_{LF} (low-frequency in-phase susceptibility) and χ_{HF} (high-frequency in-phase susceptibility). Hrouda (2011) introduced the χ_{FN} (Equation 2) parameter, which provides a similar interpretation to χ_{FD} but is less dependent on frequency, allowing for a more realistic measurement. Lastly, the low-frequency phase angle (δ_{LF}) is a useful tool for evaluating the SP/SD threshold via the χ_{ON} parameter (Equation 3) introduced by Hrouda et al. (2013). We used these parameters to verify the loss of susceptibility in our samples:

$$\chi_{FD} = \frac{\chi_{LF} - \chi_{HF}}{\chi_{LF}}, \quad (1)$$

$$\chi_{FN} = \frac{\chi_{FD}}{\ln(HF) - \ln(LF)}, \quad (2)$$

$$\chi_{ON} = 200 \cdot \pi^{-1} \tan(\delta_{LF}). \quad (3)$$

Sequentially, the cylindrical samples were sawed to extract small fragments for measurements in a vibrating sample magnetometer (Princeton Measurements Corporation MicroMag, VSM Model 2900; noise level 2×10^{-9} A m²). Magnetic hysteresis and backfield curves were performed for all samples (please refer to the public repository cited in Bellon, Williams, et al. (2023) for more details). Samples representing the overall magnetic behavior of each population were selected for the acquisition of First-Order Reversal Curves (FORCs) to further investigate the domain state and magnetic interactions of the particle assemblages.

The use and processing of FORC diagrams to examine the magnetic domain of ferromagnetic particle assemblages (for rock/environmental magnetism and paleomagnetism) have increased significantly over the last two decades (Carvallo et al., 2004, 2006; Egli, 2013; Egli et al., 2010; Heslop et al., 2020; Lascu et al., 2018; Muxworthy & Dunlop, 2002; Pike et al., 2001; Roberts et al., 2000). In our experiments, FORC measurements were carried out in cubic samples ($\approx 2\text{cm}^3$). For each sample, the routine involved acquiring 300 first-order reversal curves using the following parameters: (a) a discrete field sweep mode; (b) an averaging time of 0.5 s; (c) pauses of 1 s at the saturation, calibration, and reversal fields; (d) $B_{c_{\min}} = 0$ mT and $B_{c_{\max}} = 150$ mT; $B_{u_{\min}} = -80$ mT and $B_{u_{\max}} = +80$ mT; and a saturation field of 400 mT. Data were acquired in triplicates and further linearly combined to enhance signal/noise ratios, and finally processed through a Python-based statistical machine learning package (Heslop et al., 2020). Preprocessing involved corrections of saturation slope (at 70%), drift measurements, and normalization by mass. Even after stacking the data, its noisy nature requires a considerable amount of smoothing. For that, it was also assumed a symmetrical vertical and horizontal smoothing, limiting the maximum smoothing factor to 5.

Finally, Lowrie (1990)'s test was also carried out on representative samples by imparting orthogonal isothermal remanent magnetization (IRMs) (through a 2G pulse magnetic field inducer), with distinct field intensities of 1.2, 0.4, and 0.12 T; and further thermally demagnetizing (100–700°C) the samples to estimate unblocking temperatures of the hard (1.2–0.4 T), medium (0.4–0.12 T) and soft (<0.12 T) magnetic carriers. The remaining remanence after each demagnetizing step was then measured (also in a SQUID magnetometer).

3.2. X-Ray Diffractometry and Crystallinity Index

Authigenic growth of ferromagnetic phases due to smectite-illite transformations is among the common phenomena summoned for carbonate remagnetization. As discussed by Huggett (2005), the illitization of smectites versus depth is the most studied aspect of clay diagenesis. This process starts around 70°C and peaks around 120°C, although the geothermal gradients of a basin might lead to earlier reactions. Illitization occurs if K⁺ is available, following either of two reactions (Huggett, 2005):

- i. smectite + Al³⁺ + K⁺ → illite + Si⁴⁺ + Fe²⁺ + Na⁺ + Mg²⁺
- ii. smectite + K⁺ → illite + Si⁴⁺ + Fe²⁺ + Na⁺ + Mg²⁺

K-feldspar dissolution is the primary source of K⁺ inputs, driving the transformation of smectite to illite with mixed layers of smectite-illite (I-Sm). In early reaction stages, illite becomes randomly interstratified within the expandable layers (Lanson et al., 2009). This transformation is significant because the growth of authigenic

magnetite may involve the conversion of Fe-rich smectite to illite. To explore this possibility, selected samples were analyzed using X-ray diffractometry (XRD) to identify their solid phases, particularly clay minerals. Selection criteria included samples exhibiting the highest magnetic susceptibility, a paramagnetic contribution to hysteresis greater than 80%, and a considerable loss in magnetic susceptibility at higher frequencies (over 10%).

Samples were manually crushed using an agate mortar and pestle, then prepared for analysis in a Bruker diffractometer, ranging from 2 to 99°, in 0.02° steps (2θ) using copper source radiation (25 mA, 40 kV). Peaks were identified and matched to solid phases by analyzing both their position and lattice spacing (d-spacing).

The transformation of smectite to illite and the crystalline arrangements involved are dependent on temperature, where the crystallinity of illite increases with rising temperatures. A common method to assess paleotemperatures in illite-bearing sedimentary rocks is through KI, the Kübler index (Kübler, 1964, 1967, 1968, 1990). To determine KI, the clay fraction ($<2\ \mu\text{m}$) of the sediment is isolated, and XRD data is collected using a Cu-K α radiation source. The full width at half maximum (FWHM) of the 10° peak is then calculated. This index helps distinguish between late-diagenetic stages (toward anchizone, very low grade/incipient metamorphism) and epizone (low greenschist facies), where a smaller KI indicates higher paleotemperatures (Jaboyedoff et al., 2001). In our study, KI was used as a constraint to determine possible exposure to low-grade metamorphic conditions in the remagnetized units.

Powder samples underwent treatment in a Becker flask containing a weak acid solution composed of 2 M acetic acid and 1 M sodium acetate [4:1] (with a pH of approximately 4), following the procedure outlined in Strehlau et al. (2014). The mixture was stirred at 40°C for an hour. After neutralization, the fine fraction was isolated through decantation, and the supernatant was transferred to a plate to allow clay minerals to settle and dry, orienting platy clay minerals parallel to the glass slide to enhance basal plane peak intensities (Tohver et al., 2008). Samples then underwent a sequential XRD acquisition process: (a) initial data collection post-drying, (b) post-ethylene glycol impregnation, and (c) following calcination at 550°C. Background removal in the XRD data was performed by adjusting a forward model with linear or logarithmic decaying curves to better represent the spectrum. KI values were calculated by optimizing the parameters of a Gaussian distribution using a non-linear least squares fitting in a Python environment.

3.3. Micro-To-Nanoscale Imaging/Chemical Analysis

Using the same selection criteria as for XRD, thin sections from four samples were prepared to perform a microscale analysis of their petrographic features under natural and polarized light (See Supporting Information S1). Microscopic imaging was conducted on these sections using a HELIOS 5 PFIB CXE DUALBEAM electronic microscope, which facilitated visual analysis in secondary electron (SE) mode and chemical mapping through energy dispersive spectroscopy (EDS). This analysis primarily focused on identifying PSD-range iron oxides/sulfides within the remagnetized units and examining their spatial correlation with other mineral constituents.

Synchrotron radiation, a potent electromagnetic wave, and crucial X-ray source (Yamashita, 2003), aids in understanding material properties at a nanoscale (Duncan, 2018). Since X-rays are ionizing radiation, they can eject core electrons from atoms upon absorbing energy. Scanning the X-ray through a specific binding energy reveals a marked increase in absorption, known as a rising absorption edge, occasionally preceded by a pre-edge—characteristic of a specific core-electron binding energy and related to an element's quantum number of the excited electron (Penner-Hahn, 2003). X-ray absorption spectroscopy (XAS) encompasses two parts: X-ray absorption near-edge structure (XANES), which provides insights into the oxidation state, and the extended X-ray absorption fine structure (EXAFS), which offers details on local coordination, chemical composition, and crystal structure (Zhu et al., 2021).

Experiments were conducted at the Coherent X-ray Nanoprobe Beamline (CARNAÚBA) of SIRIUS, the Brazilian Synchrotron Facility (Oliveira et al., 2014), which offers a spectroscopic range of 2.05–15 keV (Tolentino et al., 2017). Data acquisition occurred via an environmental in-air nanoprobe (TARUMÃ), suitable for tender-to-hard X-ray sub-micro analysis. Representative thin sections from the BB, IR, and GC groups were carefully positioned to align the beam with selected regions (approximately 2 mm²). The samples underwent raster-scanning to capture two-dimensional data (Tolentino, 2021). For X-ray fluorescence (XRF) data, Gaussian distributions were fitted to the logarithm of peak intensity versus energy, using mean values μ to qualitatively

determine element concentrations within specific areas. X-ray absorption spectroscopy (XAS) data was collected in fluorescence mode at the Fe K-edge (activation energy, $E_0 \approx 7112$ eV), calibrating the monochromator with metallic Fe-foils. Each sample underwent three sequential scans to optimize the signal-to-noise ratio. The normalization procedure followed in this study aligns with those used in specialized software (Ravel & Newville, 2005). Comparative XAS data for α -Fe₂O₃, γ -Fe₂O₃, and Fe₃O₄ (hematite, maghemite, and magnetite, respectively) were sourced from Piquet et al. (2014), and FeS₂ (pyrite) from Ravel (2013), to benchmark against our experimental findings.

3.4. Thermogravimetric Analysis Coupled to a Quadrupole Mass Spectrometer (TGA-QMS)

To better correlate the presence of hydrocarbon and sulfur in samples of the Mirassol d'Oeste and Guia Formation, thermogravimetric analysis coupled to a Quadrupole Mass Spectrometer (TGA-QMS) was performed under constant synthetic air flow (40 m/min) on samples from the Guia Formation over the Amazon craton (GT) and its underlying dolostones from the Mirassol d'Oeste (MO_{transition}); as well as bitumen-poor samples from the dolostones immediately above the diamictites of the Puga formation (MO_{base}). With this analysis, we intend to understand the differences in the amount of organic matter (CO₂) and sulfur content (SO₂, SO₃), by checking the mass loss as temperature increases.

4. Results

4.1. Rock Magnetism

4.1.1. Frequency Dependent Magnetic Susceptibility

Samples from the three studied basins exhibited a loss in magnetic susceptibility from low to high frequencies, with the displacement in susceptibility distribution visible in the respective boxplots for each group (Figure S1 in Supporting Information S1). Notably, the calculated χ_{FD} values for most samples are significantly large (>10%), though some from the Irecê samples (IR) are below 5% (Figure S1h in Supporting Information S1). The Araras Group samples, particularly those from the Guia Formation, showed the most substantial loss of susceptibility, as reflected in their χ_{FN} values (Figures S1i and S1j in Supporting Information S1). Two samples from the GT and GC groups displayed extreme susceptibility loss (>30%, see the Figures S1i and S1j in Supporting Information S1). Given that χ_{FN} and χ_{ON} parameters are expected to be equivalent, a linear trend was anticipated. However, GT and GC samples exhibited anomalous responses across different frequencies, yet they maintained a linear relationship between χ_{FN} and χ_{ON} parameters, as discussed by Hrouda et al. (2013). Diamagnetic materials like calcite can increase δ_{LF} , leading to large χ_{ON} values. Nonetheless, the correlation between χ_{FN} and χ_{ON} values allowed for a linear regression through least squares fit across all groups, with determination coefficients $R^2 > 0.79$. A higher dispersion in χ_{FN} versus χ_{ON} values was particularly evident in the Irecê (IR) samples, possibly due to the presence of paramagnetic phases decreasing δ_{LF} or measurements near the experimental resolution.

Remagnetized carbonate rocks typically exhibit χ_{FD} values greater than 5% (Font et al., 2006), indicative of a significant contribution from superparamagnetic grains. The χ_{FN} values of remagnetized units confirm a notable loss in magnetic susceptibility. Interestingly, the basal samples from Mirassol d'Oeste (our control test) also demonstrated a considerable loss of susceptibility (>5%), mirroring the behavior observed in the IR samples.

4.1.2. ARMs, Magnetic Hysteresis, and Backfield Curves Parameters

Apart from a few samples, the general behavior of anhysteretic remanent magnetization (ARM) curves (Figure S3 in Supporting Information S1) is consistent within the same geological unit. Some samples from the Bambuí and Irecê units appear not to reach saturation at 100 mT. Notably, the Bambuí samples exhibit a shallower slope in their magnetization curves compared to those from Irecê, suggesting the presence of more coercive phases in the latter. Conversely, other samples from these units closely resemble those from the Guia Formation, achieving most of their magnetization by 70 mT. In the Araras Group, samples from both the Guia Formation and Mirassol d'Oeste approach saturation around 100 mT. However, the magnetization curves of Mirassol d'Oeste samples have a steeper slope, indicating a greater contribution from low-coercivity minerals. The gradient of the ARM acquisition curves across all units reveals that most magnetization is acquired at coercivities below 20 mT, typically indicative of magnetite. Interestingly, these samples (BB, IR, GC, and GT) also display coincident peaks

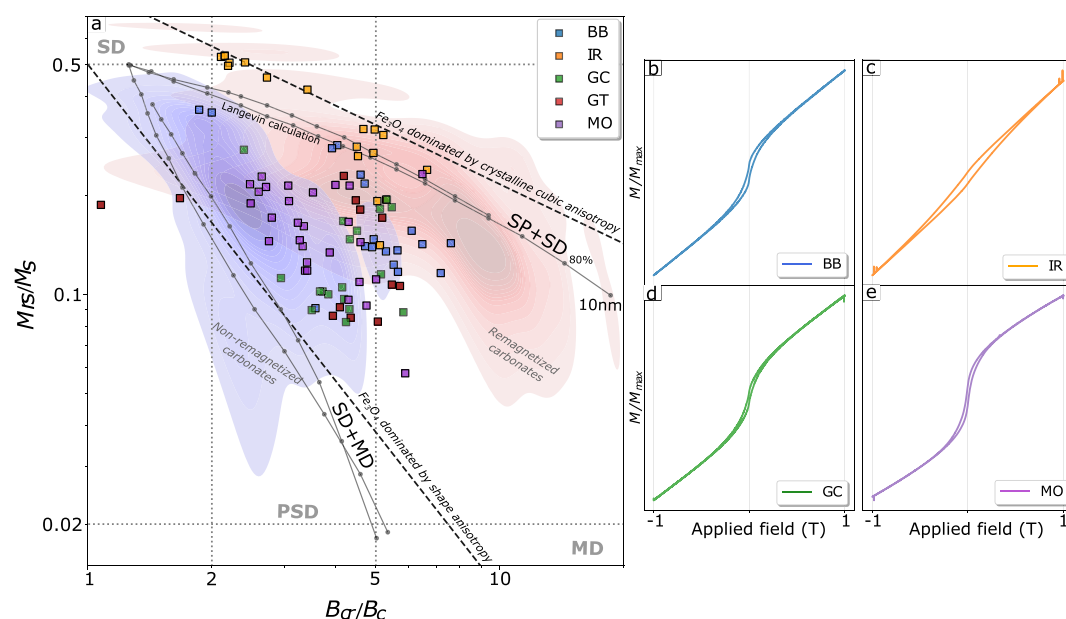


Figure 3. (a) Bilogarithmic Day-Dunlop plot compiling data from magnetic hysteresis and backfield curves from the analyzed samples. Solid black lines are the mixtures of multidomain (MD) + single-domain (SD), or a mixture between single-domain (SD) and superparamagnetic populations of magnetite (Dunlop, 2002). Solid gray lines are the theoretical trends followed by a single-sized population of magnetite controlled by shape anisotropy (intercept at 0.5 in the M_{rs}/M_s -axis) and controlled by crystalline cubic anisotropy (intercept at 0.89 in the M_{rs}/M_s -axis) (Jackson, 1990; Parry, 1982). The blue and red contours represent density frequencies of non-remagnetized/remagnetized carbonates, respectively (Jackson & Swanson-Hysell, 2012). Plots on the right are representative magnetic hysteresis of each studied unit. Remagnetized carbonates yielded distorted loops, for which Bambuí (b) and Guia samples (d) are mostly wasp-waisted and Irecê samples are potbellies (c). Mirassol d'Oeste samples (e) are ordinary low coercivity loops expected for magnetite-bearing rocks.

in coercivities around 40 mT, which are absent in the dolomites of the Mirassol d'Oeste Formation. This behavior suggests the potential presence of multiple remanence-bearing minerals in the remagnetized units.

Uncorrected hysteresis analysis of the samples reveals a significant involvement of paramagnetic materials, with over 75% of the samples exhibiting a paramagnetic contribution of approximately 80% at the maximum applied field (Figure 3b–3e). Furthermore, the analysis of the gradient of the irreversible loop performed by Bellon, Trindade, and Williams (2023) and Bellon, Williams, et al. (2023) shows a linear component in magnetization, attributed to the paramagnetic contribution, resulting in a positive basal displacement of the gradients. In some instances, this paramagnetic contribution can surpass the ferromagnetic contribution, reaching up to 99% of the sample saturation magnetization, indicating a substantial presence of iron-bearing silicates, especially clay minerals, in these carbonate rocks.

When corrected for paramagnetic/diamagnetic contributions, distorted hysteresis loops become more apparent in the remagnetized carbonates, with saturation not achieved at fields below 100 mT in most samples. Bambuí samples typically display a wasp-waisted hysteresis loop (Figure 3b), indicative of mixed magnetic carrier populations with distinct coercivities or a combination of superparamagnetic and single-domain behaviors. In contrast, hysteresis from Irecê samples resembles potbellies (wider middles and curved shoulders, Figure 3c). While Bambuí samples suggest the presence of magnetite, the larger coercivities observed in some Irecê samples indicate the presence of minerals with higher coercivities, though magnetite in the same samples is not ruled out. Samples from the Guia (Figure 3d) and Mirassol d'Oeste (Figure 3e) formations exhibit similar magnetic hysteresis, but distorted loops are more frequent in Guia samples. No significant differences are observed between the deformed and undeformed terranes (GC and GT samples, respectively), with potbellies absent but wasp-waisted hysteresis frequently occurring.

One method to interpret results from magnetic hysteresis involves using these as bulk indicators of the magnetic domain state. Although other methodologies such as FORC diagrams also infer domain states and will be discussed later, remagnetized carbonates are known to exhibit specific trends on the Day plot (Day et al., 1977).

Initially, these trends were attributed to magnetocrystalline cubic anisotropy (Jackson, 1990). However, this hypothesis was based solely on the intercept value of a power-law trend. Subsequent experiments have demonstrated that, in reality, shape anisotropy governs the magnetic properties of magnetite in remagnetized carbonate rocks (Jackson & Swanson-Hysell, 2012), and that abnormal hysteresis ratios should be correlated to mixtures with SP grains (or different magnetic minerals).

Samples from the Bambuí and Araras Groups generally do not conform to the single-sized shape-controlled anisotropy nor follow the North American carbonate trend (Figure 3a), which is considered a “false negative” in magnetic fingerprinting. This indicates that while samples are paleomagnetically remagnetized, their bulk hysteresis properties do not align with the expected fingerprint. Conversely, most of the Irecê samples align closely with this trend and appear to follow it.

Domain states of magnetic particles are dependent on size and shape constraints. The superparamagnetic threshold (d_s) and critical single-domain size (d_0) vary among different materials and even change with the shape of the same material (Butler & Banerjee, 1975). Most magnetic particles in rocks do not conform strictly to MD or SD theory, often exhibiting a non-uniform magnetic state classified as PSD (Nagy et al., 2017). Our data predominantly fall within the PSD field, though some samples from the Mirassol d'Oeste Formation could be interpreted using the non-linear mixing theory from Dunlop (2002).

Previously, unmixing methods were applied by Bellon, Trindade, and Williams (2023) and Bellon, Williams, et al. (2023) to discern susceptibility components within distorted hysteresis loops from the Salitre and Sete Lagoas Formations. Despite the inherent limitations of any parametric unmixing method, which relies on the model's capacity to explain a given phenomenon, the analysis demonstrated that potbellies and wasp-waisted features in BB and IR samples could arise without a substantial contribution from SP particles. Instead, these features were attributed to the presence of different coercivity components corresponding to distinct minerals. Paleomagnetic data already suggest the presence of both monoclinic pyrrhotite and PSD magnetite in the remagnetized units, yet their placement in the Day plot poses challenges in correlating them to specific domain states. It was noted, however, that mixing scenarios involving SP + SD, PSD + SP, and similar combinations could generate a variety of distributions below the $0.5 M_{rs}/M_s$ threshold, as discussed by Dunlop (2002). Consequently, the mixing of distinct magnetic populations in remagnetized carbonates can exhibit considerable dispersion.

4.1.3. FORC Diagrams

Most of the Bambuí samples (Figure 4a') exhibit a significant contribution along the coercivity axis (B_c), with minimal contribution to the interaction axis (B_u), typical of non-interactive single-domain (SD) particles (Roberts et al., 2000, 2022). The central-ridge contribution is commonly associated with biogenic magnetites, such as that from magnetotactic bacteria in pelagic sediments, characterized by its sharpness due to minimal magnetostatic interactions (Roberts et al., 2011). Ultrafine authigenic magnetic particles might also influence the central ridge response, though this effect depends on the dispersion within the particle matrix (Egli et al., 2010). Highly dispersed pedogenic SD magnetite, contributing to the lack of magnetostatic interactions, has been suggested by Geiss et al. (2008). The distribution's center in Figure 4a' is close to the origin on the B_c axis and extends toward higher field values, likely indicating the presence of a particle assemblage with varied coercivities. This distribution could be attributed to a range of SD/vortex-state particles of magnetite and pyrrhotite sparsely distributed within the carbonate matrix.

Irecê samples exhibit a range of coercivity values. FORC diagrams for these samples are typically noisy, even after linearly combining multiple stacks of the same samples, resulting in FORCs that resemble potbelly like loops (Figure 4b). Smoothing and artifacts generated during processing are evident as medium-intensity contributions distant from both the central ridge and the origin of the B_u -axis (Figure 4b'). Nonetheless, the primary distribution remains centered along the coercivity axis, similar to the Bambuí samples.

Guia Formation samples from both Terconi and Cáceres regions display similar hysteresis/backfield parameters, with FORC diagrams showing no clear magnetic differentiation between the terranes. The main response is typically asymmetric, centered on the B_c -axis with slight spreading toward the interaction axis, indicative of a PSD state. Increasing grain size within the PSD threshold tends to reduce coercivity, leading to a divergence toward the B_u -origin and a more MD-like appearance (Roberts et al., 2000, 2014). However, some samples

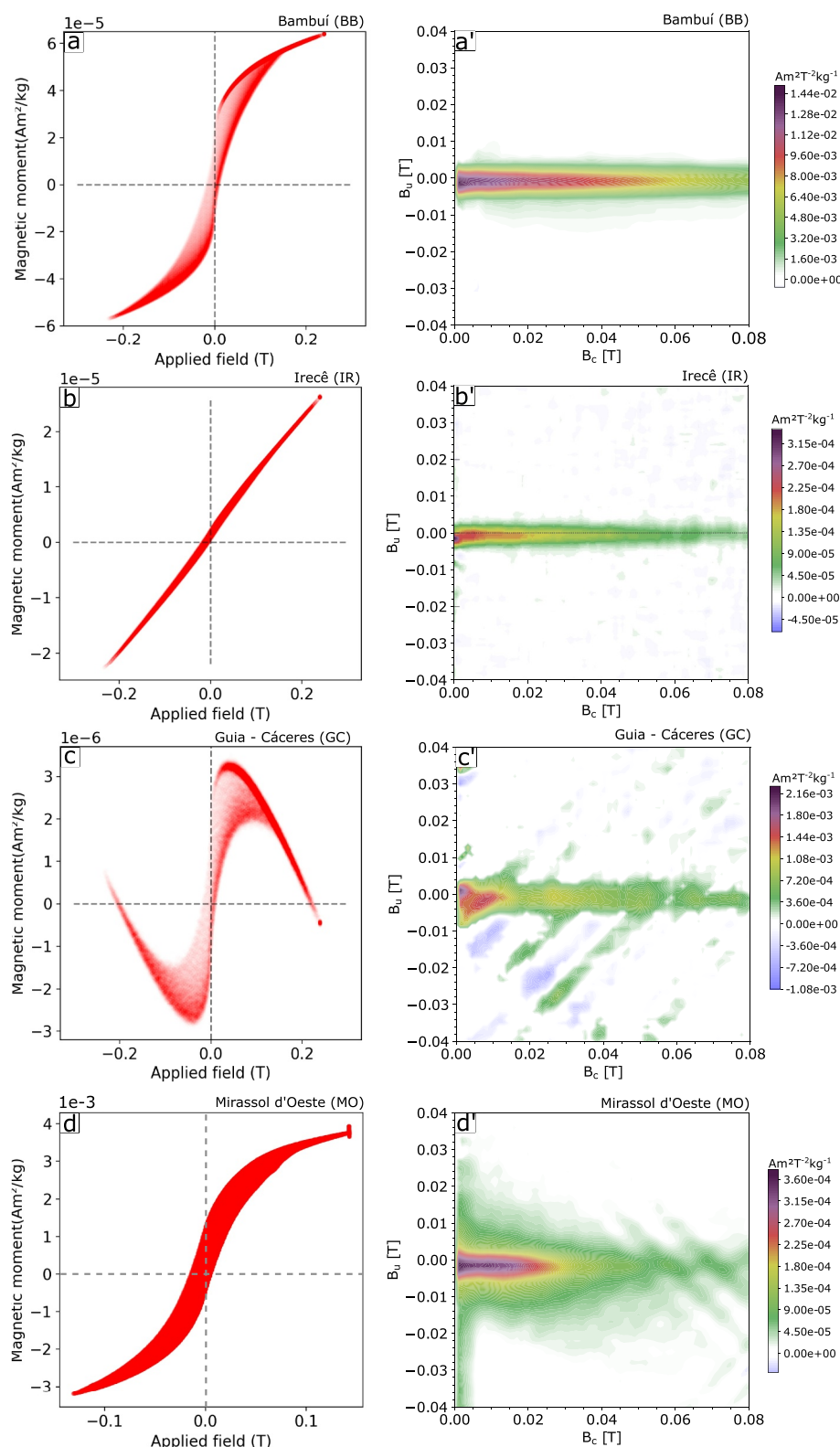


Figure 4. First-order reversal curves (FORC) of representative samples of both remagnetized (a–c) units and non-remagnetized unit (d). These FORCs are linear combinations (stacks) of sequential acquisitions to improve the signal-to-noise ratio. The respective FORC diagrams (a'–d') were processed through the FORCsensei package and optimized to a smoothing factor of 5. Geological units are indicated in the upper right corner of each plot.

primarily show a major distribution along the coercivity axis, akin to the Bambuí samples. A few samples from the Guia Formation (both Terconi and Cáceres) exhibit significant diamagnetic contributions due to the carbonate matrix. Despite this, the ferromagnetic contribution remains distinguishable (Figure 4c), but diamagnetic correction results in diagonal positive/negative intercalation of artifacts (Figure 4c'). Nevertheless, the dominant contribution to the coercivity axis is apparent, likely due to non-interactive single-domain grains.

FORC diagrams of the non-remagnetized unit of the Araras Group (Mirassol d'Oeste) generally exhibit PSD-like behavior, similar to the major response seen in Guia Formation samples, with diagonal artifacts occasionally resulting from paramagnetic corrections. Notably, a few diagrams show significant contributions near the origin along the B_H -axis, suggesting that MD particles may also be influencing their magnetic spectra (Figure 4d').

Overall, the remagnetized carbonates under study display consistent features in their FORC diagrams. The pronounced central ridge indicates the presence of stable SD/PSD grains across various grain sizes and hints at the potential existence of superparamagnetic grains, evidenced by extensions toward zero along the B_c -axis. While FORC diagrams are valuable for assessing the magnetic properties of rock assemblies, they reflect the combined response of all ferromagnetic particles within the samples. Differentiating individual magnetic contributions in samples with complex magnetic mixtures remains challenging. Although methods for unmixing FORC components are documented (Harrison et al., 2018), their successful application requires well-defined particle assemblages, which are not typically found in these remagnetized carbonates.

4.1.4. Lowrie Test

In the Lowrie test (Figure 5), the medium and hard-coercivity components of sample BB-2 (Figure 5a) exhibit unblocking temperatures near 350°C, with a residual intensity of less than 10% that is completely decayed at 450°C, indicating the presence of pyrrhotite and a smaller amount of magnetite. Meanwhile, the soft fraction smoothly decays up to 550°C, which is typical of MD-magnetite. In some other samples (e.g., BB-16, Figure 5b), pyrrhotite appears to be absent, as all three components smoothly decay to zero between 500 and 550°C. Irecê samples with magnetic hysteresis showing coercivities larger than 100 mT exhibit all three components completely decaying at 700°C, indicative of hematite, with no indications of the presence of magnetite or pyrrhotite (e.g., IR-6, Figure 5d). However, these samples are much less common than those with a coercivity of remanence smaller than 100 mT (e.g., IR-11, Figure 5c), which display two components: one around 350°C (pyrrhotite) and another that slowly demagnetizes completely around 500°C (magnetite). The soft component of sample IR-11 should also be associated with magnetite. These samples exhibit signatures more similar to those observed in the Bambuí samples.

Sample GT-11 (Figure 5e) exhibits a slower decay of the hard component up to 250°C, followed by a steeper decay up to 350°C, and then it smoothly demagnetizes until 550°C. In this case, the lower decay temperatures could be associated with maghemite and/or pyrrhotite, while the higher blocking temperature (along with the soft and medium components) represents magnetite. For sample GC-2 (Figure 5f), the hard and medium components slowly decay up to 400°C, but only completely demagnetize at 500°C (together with the soft component, which linearly demagnetizes up to this temperature). This behavior is likely related to maghemite/oxidized magnetite (lower blocking temperature) and magnetite (higher blocking temperature).

The medium and hard components of sample MO-2 (Figure 5g) exhibit rapid decay from 100 to 150°C, followed by linear decreases up to 580°C. This rapid decay could indicate the presence of a higher coercivity mineral, such as goethite. Although there is a component of the soft fraction that demagnetizes at 350°C (MO-2 sample, Figure 5c), it differs from Bambuí and Irecê samples in terms of coercivity (as in those samples, the pyrrhotite component is associated with medium and high coercivity components). However, most of the samples are dominated by magnetite, displaying behavior more similar to that of the MO-22 sample (Figure 5h), with medium and hard components smoothly demagnetizing until 580°C and a soft component linearly demagnetizing up to 450°C, followed by slow demagnetization up to 550°C.

4.2. XRD

Samples from the Bambuí (Figure 6a) are essentially composed of calcite, but the diffraction patterns also indicate the presence of quartz, chlorite, and possibly feldspars (both K-feldspar and plagioclase), and a minor presence of dolomite. The mineralogical composition of samples from Irecê (Figure 6b) closely resembles that of the Bambuí

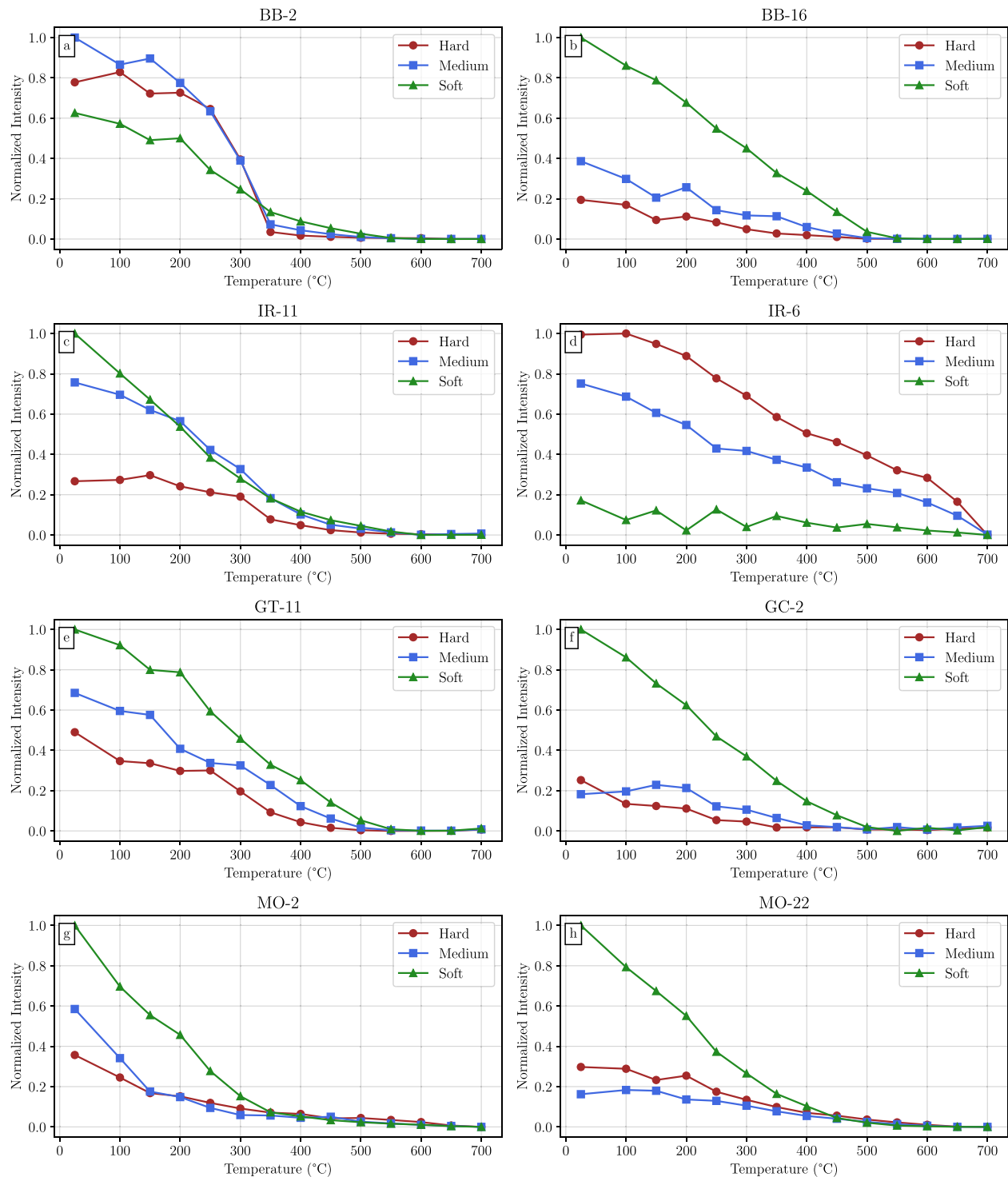


Figure 5. Results for the Lowrie test, which involves imparting an isothermal remanent magnetization (IRM) in three orthogonal directions: 1.2 T (hard), 0.4 T (medium), and 0.12 T (soft). Subsequently, samples undergo stepwise thermal demagnetization to characterize how each coercivity component behaves. Sample names are indicated in the upper part of each subplot.

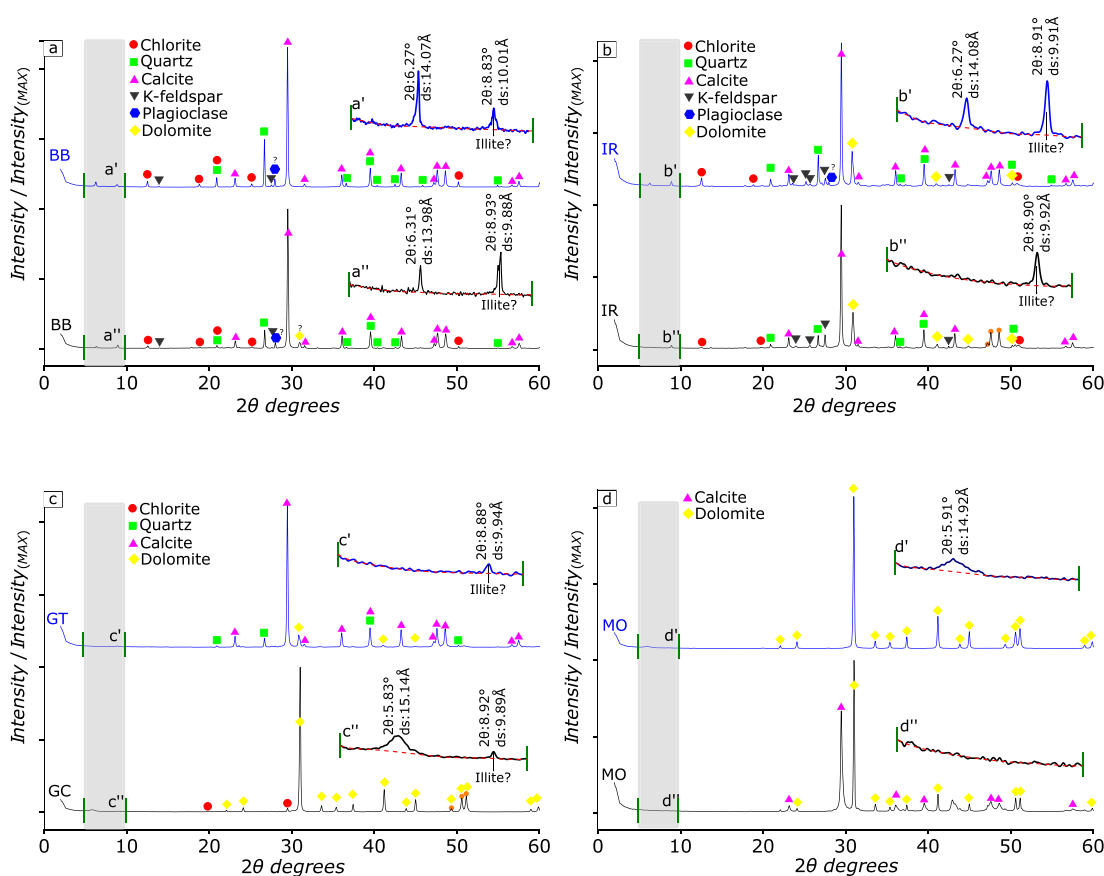


Figure 6. XRD diffractograms of samples from the Bambuí (a), Irecê (b), Guia (c), and Mirassol d'Oeste formation (d). Diffractograms are colored following the sample names (two per unit). The shaded gray marks the expanded areas between 4 – 10° (2θ) shown in the upper right of each diffractogram (e.g., a' and a'' are the expanded areas for BB-6 and BB-12 samples, respectively) to highlight the occurrence or lack of the 10Å peak of illite around 8.9° (2θ).

samples. However, the presence of dolomite and K-feldspar is more strongly marked. The Guia Formation samples (Figure 6c) exhibit greater variability, depending on the group (GT, GC), as the majority of the diffraction data from the Cáceres region is associated with dolomite, while from Terconi, it is related to calcite. Samples from the lowermost stratum of the Araras Group, the Mirassol d'Oeste formation (Figure 6d), are almost monomineralic (in terms of major constituents) and composed of dolomite and calcite.

When chlorite peaks were observed, we conducted further investigation using ethylene glycol. This step was necessary because smectites have a similar d-spacing (14Å) to chlorite, which can vary due to liquid-phase adsorption (9.6 – 21.4Å) (Tucker, 2001). Furthermore, if illite is authigenic, the transformation may not have been complete, resulting in residual smectite that remains either isolated or intercalated with illite layers. This underscores the necessity of conducting such an analysis.

A common behavior for Bambuí, Irecê, and Guia Formation samples is the occurrence of a peak around 8.9° (2θ). These peaks have a very small intensity compared to the major constituents of the samples but are distinct from the background signal (Figure 6). Lattice spacing values of such peaks are near 10Å, which is an indication of the presence of illite (Patarachao, 2019; Tohver et al., 2006). Interestingly, none of the samples from the Mirassol d'Oeste formation showed the presence of such a peak, indicating its absence or only a trace amount of concentration.

Upon isolating the clay fraction data, the optimization of Gaussian curves returned a good fit around the illite peaks at approximately 9° (2θ) for both the Sete Lagoas and Salitre Formation samples. This resulted in similar Kübler Index (KI) values of 0.14° and 0.13°, respectively, as illustrated in Figures 7a and 7b. These values

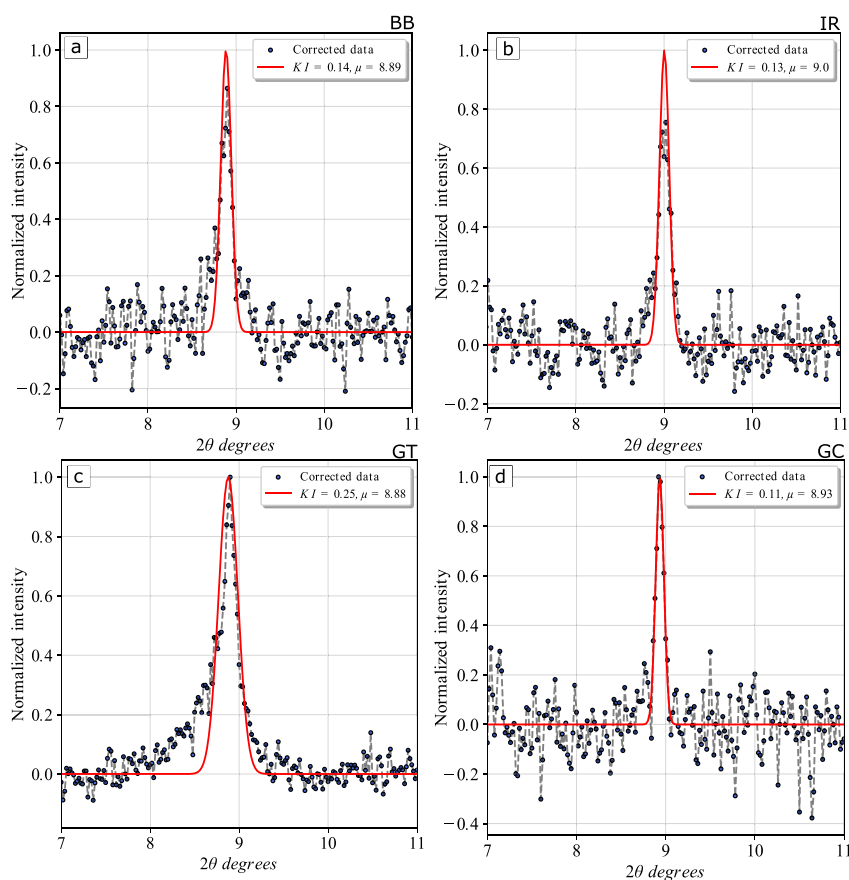


Figure 7. XRD experiments after carbonate dissolution of samples from Sete Lagoas (a), Salitre (b), and Guia formations (c, d). Corrected data refers to XRD background subtraction. Fitting of Gaussian components at the illite peaks ($\approx 9^\circ$) was performed to sequentially calculate the Kübler index ($2\sqrt{2\ln 2} \cdot \sigma$), where σ is the dispersion around the mean.

indicate a high crystallinity index, consistent with the low greenschist metamorphic facies (epizone) (Mählmann & Frey, 2012). Despite recognized deformation along the borders of the Bambuí Group due to the Araçuaí and Brasília belts (Moreira et al., 2020), the sampled area derives from a stable cratonic region (Chemale et al., 1993).

These findings suggest that, although the area was not tectonically disturbed, it could have been exposed to temperatures as high as 350°C , which is the upper limit for the epizone. Such conditions, far removed from diagenetic environments, imply that if the correlation between remagnetization and illite generation is confirmed, the remanence of Bambuí rocks is likely non-diagenetic. Smectite-illitization requires not only temperature but also an input of K^+ . The dissolution of K-feldspars in these rocks could provide an in situ potassium source for illitization, although hydrothermal percolating fluids might also trigger illitization. In such context, $\delta^{13}\text{C}$ and $\delta^{18}\text{O}$ data of samples from the Salitre Formation have been interpreted as indicative of the percolation of external hydrothermal fluids (Couto, 2020).

Ethylene glycol treatment for the BB sample slightly increases the full-width at half maximum (FWHM) but causes considerable displacement after calcination at 550°C (Figure S4a in Supporting Information S1). Ethylene glycol penetrates smectite's interlayer spaces, leading to the formation of a two-layer structure (Szczerba et al., 2014), indicating that an I-Sm structure persists in the Bambuí-sample. This is supported by a crystalline index pointing to an ordered sequence mostly composed of illite layers (Lanson et al., 2009). For the IR sample, the illite peak exhibits an almost negligible change, indicating a higher purity of illite content. Additionally, XRD data for bulk samples show peaks at 6.27° for the Sete Lagoas and Salitre Formations. If related to smectite, this would contradict the presence of such crystalline illites. However, none of their peaks (of BB and IR samples)

swelled to 17 Å with ethylene glycol treatment, as would be expected if these peaks were attributed to smectite; instead, they are interpreted as chlorite peaks (Szczerba et al., 2014).

For the Guia Formation, results differ between the two terranes: samples from the Amazon Craton (Terconi quarry, GT) yielded a Kübler Index (KI) value of 0.25° (Figure 7b), while those from the Paraguay belt (Cáceres, GC, Figure 7d) recorded a significantly lower index of 0.11°. The GT samples suggest transitional conditions from mid-to-high anchizone, indicative of incipient metamorphic conditions, whereas the GC samples align with conditions similar to those of the Salitre and Sete Lagoas Formations. These findings align with the expected illite crystalline indexes transitioning from the Amazon Craton to the Cáceres region (Alvarenga, 1990). Post-ethylene glycol saturation, the GT illite peaks indicate an I-Sm structure (Figure S2c in Supporting Information S1), while the GC sample exhibits a response more akin to the Bambuí samples, showing no considerable changes. Unfortunately, the previously observed peak at 15.14 Å (Figure 6c) was not detected after carbonate dissolution.

The presence of illite in all remagnetized units not only supports a robust hypothesis for the process responsible for remagnetizing carbonate units across West Gondwana but also provides insights into the paleotemperature conditions these rocks experienced. This is particularly relevant as these rocks contain different magnetic minerals with statistically indistinguishable paleomagnetic directions and because temperatures consistent with the anchi/epizone are kinetically favorable for the formation of monoclinic pyrrhotite, as observed in the Salitre, Sete Lagoas, and Guia formations.

4.3. Microscopic Data

4.3.1. Scanning Electron Microscopy With Energy Dispersive X-Ray Spectroscopy (SEM-EDS)

Our first textural observation is the lack of microporosities, suggesting a high degree of compaction and partial recrystallization under low-grade metamorphic conditions, as inferred from their tenacity during sample preparation. The largest concentrations of Fe are found in regions composed solely of this element (excluding oxygen), suggesting that iron oxides are the dominant phases. Large anhedral (likely MD) grains are scattered within the carbonate matrix. Petrographic confirmations (see Supporting Information S1) show that most of the carbonate material in all studied samples is calcite, with dolomite more prevalent in samples from the Salitre Formation. A significant presence of aluminosilicates is observed across the three remagnetized units, which, based on petrographic and XRD data, are likely smectite, illite, chlorite, or K-feldspar.

The aluminosilicates are categorized based on their elemental composition: (R_i) regions containing Si, Al, Fe (or Si and Al only), but depleted in Mg and K (Figures 8a and 8c); (R_{ii}) regions with Si, Al, Mg, Fe, but depleted in K (Figure 8b); and (R_{iii}) regions containing Si, Al, K, but depleted in Mg and Fe (Figure 8b). Both chlorite and smectites, which may include Fe and Mg in their structure, correspond to regions (R_i) and (R_{ii}). In contrast, K-feldspar and illite match the chemical signatures of the region (R_{iii}), though I-Sm structures could present all these elements depending on the illitization level.

A strong spatial correlation exists between aluminosilicates and iron oxides and sulfides. For example, the proximity of clays to iron oxides in Figure 8b might directly indicate the crystallization of magnetic minerals due to smectite illitization. The texture of iron oxide particles is typically rounded, with subhedral habits observed and diameters smaller than 1,000 nm. Iron sulfides usually appear as small isolated particles (not larger than 2 μm), especially in the Bambuí (Figure S5a in Supporting Information S1) and Irecê (Figure S5a in Supporting Information S1) samples. Framboids are frequent in the Guia Formation, appearing as euhedral cubic crystals (<1,000 nm) between clay layers (Figure S5c in Supporting Information S1). In this scenario, percolating hydrocarbons might trigger smectite-illitization by transporting K^+ from dissolved K-feldspars, and with substantial inputs of hydrogen sulfide, promoting the nucleation of pyrite and its framboidal aggregation.

4.4. Synchrotron X-Ray Fluorescence (XRF) and X-Ray Absorption Spectroscopy (XAS)

In all the samples we studied, calcium, iron, and potassium have been identified as the primary constituents in the regional X-ray fluorescence (XRF) spectrum, which refers to the analysis of the average elemental composition within the current 2D field of view (Figure S6d in Supporting Information S1). Dark regions within the maps, composed of elements invisible to the detectors, are likely silicon, given (a) its emission energies ($K\alpha \approx 1739.98$ eV) fall below the spectroscopic range of the CARNAÚBA; (b) the thin sections are attached to a silica plate (1 cm²); and (c) the high-energy X-ray beam penetration depth fully traverses the 30 μm thickness of the samples,

differing from other analytical methodologies like ordinary EDS, which receives signals not only from surface particles but also from those in-depth (Figures S6a–S6c in Supporting Information S1).

Detecting “iron islands” is crucial as a marker of the presence of possible ferromagnetic grains, previously identified through magnetic mineralogy experiments, as most of the potassium is spatially correlated with these occurrences as well. Compared to previous XRD and petrographic data, potassium is likely associated with either the clay minerals from the rock matrix or K-feldspar.

XAS data for a Bambuí sample (Figure 9a) reveals a rounded particle with decreasing iron concentration from the center toward the border. Its pre-edge region in XAS (Figure 9a'), also present in other samples analyzed by XAS, results from $1s \rightarrow 3d$ transitions in the K-edge of first-row transition metals (Penner-Hahn, 2003; Shulman et al., 1976). The rising-edge region does not completely match the spectrum of bulk phases of magnetite, maghemite, or hematite, as energy shifts of the absorption threshold due to distinct Fe-O bond lengths affect the local geometry and influence the chemical sensitivity of XANES (Piquer et al., 2014). For this specific particle, the rising edge and central peak are more consistent with maghemite. Given the iron gradient from the center to the border (Figure 9a), this suggests a core-shell structure, possibly with a preserved magnetite core surrounded by a maghemite rim. This particle would thus be within the theoretical PSD range for magnetite, while its morphology possibly indicates a diagenetic origin. This finding represents an isolated ultrafine particle in the rock matrix contributing to a central ridge in FORC diagrams, and importantly, it's a direct observation of a magnetic mineral within the stable PSD range (Nagy et al., 2017), capable of maintaining a very stable remanence and likely a product of alteration chemical remanence (a-CRM) following in situ crystallization.

For the example shown for the Irecê sample (Figure 9b), subhedral and irregularly shaped particles approximately 1,000 nm in diameter exhibit a XANES spectrum where the rising edge and central peak match with magnetite. These nanoscopic particles are dispersed within an iron-bearing matrix, possibly iron-bearing silicates. The narrow peak observed (Figure 9b'), known as a “white-line” feature, indicates intense absorption in the near-edge region (Penner-Hahn, 2003). This result is significant as it demonstrates that alongside pyrrhotite, which may contribute to the remanence of these rocks, very fine magnetite particles also exist in the Salitre rocks. This finding is interpreted as a probable result of growth chemical remanence due to its chemical purity. Yet again, these particle sizes are within the stable range of PSD grains, which predominantly bear stable remanence.

For the Guia sample, although iron oxides are more common, a globular-shaped particle (Figure 9c) yields an XAS spectrum consistent with pyrite (FeS_2) (Figure 9c'). Ahead of the pre-edge region, an increase in energy before the main peak, common in nanoparticulate phases of FeS, is observed (Matamoros-Veloza et al., 2018). The match between the reference material and the data supports the interpretation of this particle as a pyrite framboid, which is common in sedimentary systems with hydrocarbons (Machel, 2001).

Collectively, the use of highly precise XRF and XAS data forms a powerful tool for investigating remanence-bearing minerals in weakly magnetic rocks. In addition to identifying grains falling within the vortex state dimensions for magnetite, as observed by Nagy et al. (2019a), our analysis reveals even smaller mono-elementary regions enriched in iron dispersed throughout the samples (as in Figure 9b). Although the morphology of these smaller grains is challenging to discern due to experimental constraints, they likely represent even smaller particles within the thin section, approaching the limits of PSD with SD states.

4.5. TGA-QMS

The analysis of samples from the Araras Group reveals further compositional complexities due to hydrocarbon percolation. Samples from Mirassol d'Oeste notably exhibit stable detrital remanent magnetization (DRM) components (Font et al., 2005; Trindade et al., 2003), in contrast to the predominantly secondary remagnetized components observed in the overlying Guia formation. This variability might be influenced by processes triggered by hydrocarbon percolation Júnior et al. (2016), highlighting the need to determine the levels of hydrocarbons and volatile content in these samples. We employ TGA-QMS (Thermogravimetric Analysis coupled to a Quadrupole Mass Spectrometer) to quantify critical volatile components such as CO_2 , SO_2 , SO_3 , and H_2O .

H_2O is lost across the entire range of temperature (30°C–600°C) for all samples, following a linear trend attributed to the loss of structural water (OH) from clay minerals. The most significant mass loss event relates to CO_2 release, occurring similarly for samples enriched in bitumen (Figure 10, c'), with major peaks at 50°C and approximately 550°C. Thermal decomposition of calcite only begins around 700°C (Karunadasa et al., 2019),

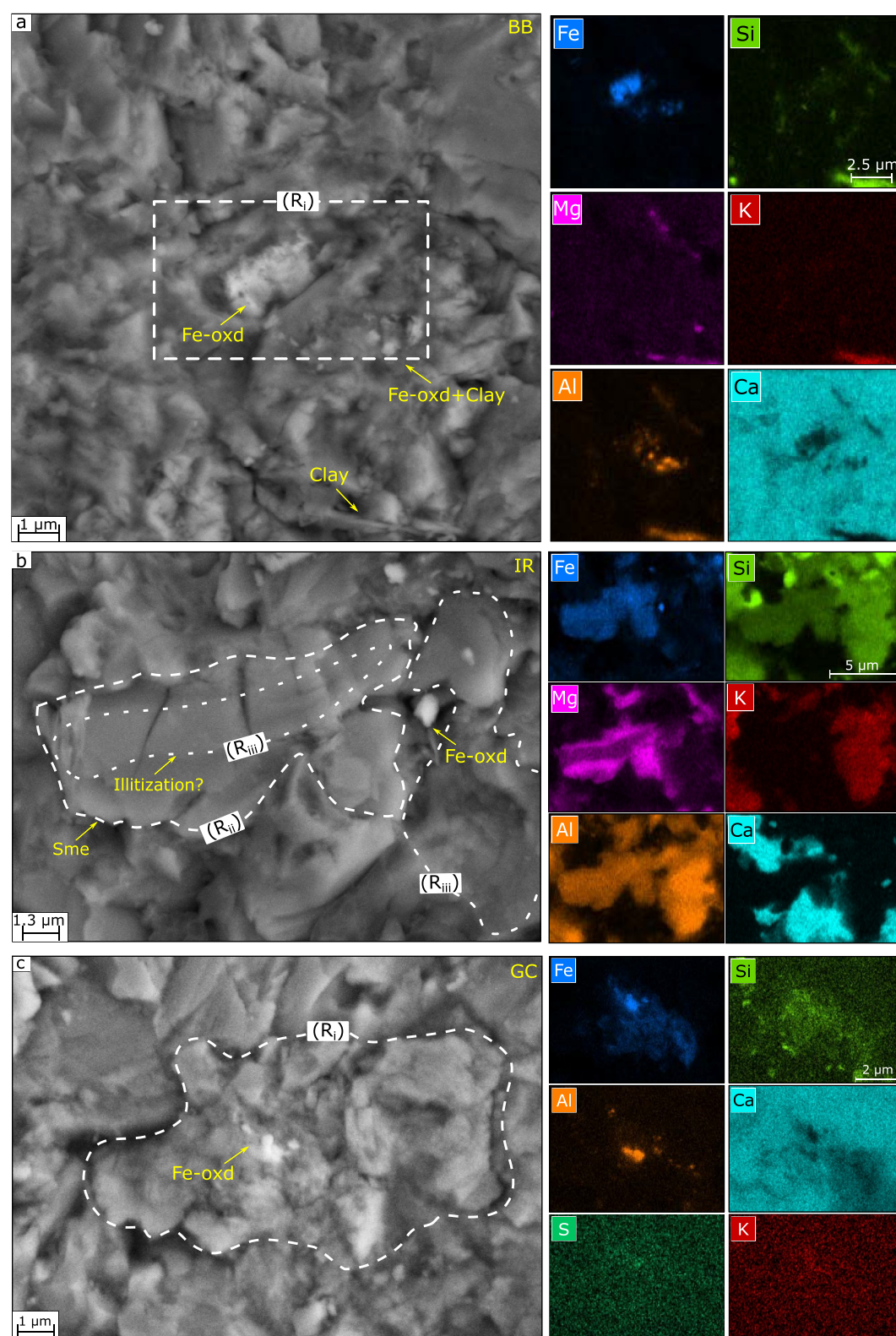


Figure 8. SEM (SE-mode) images showing the occurrences of iron oxides (Fe-oxd) near aluminosilicates in samples of the Sete-Lagoas Formation (a), Salitre Formation (b), as well as in Guia Formation (c). The right-column images are EDS chemical maps with the same target in the left column. R_i , R_{ii} , and R_{iii} highlight the chemically different occurrences of the aluminosilicates (smectite, illite, chlorite) and/or K-feldspar (check SEM section for clarity). Sme: smectite.

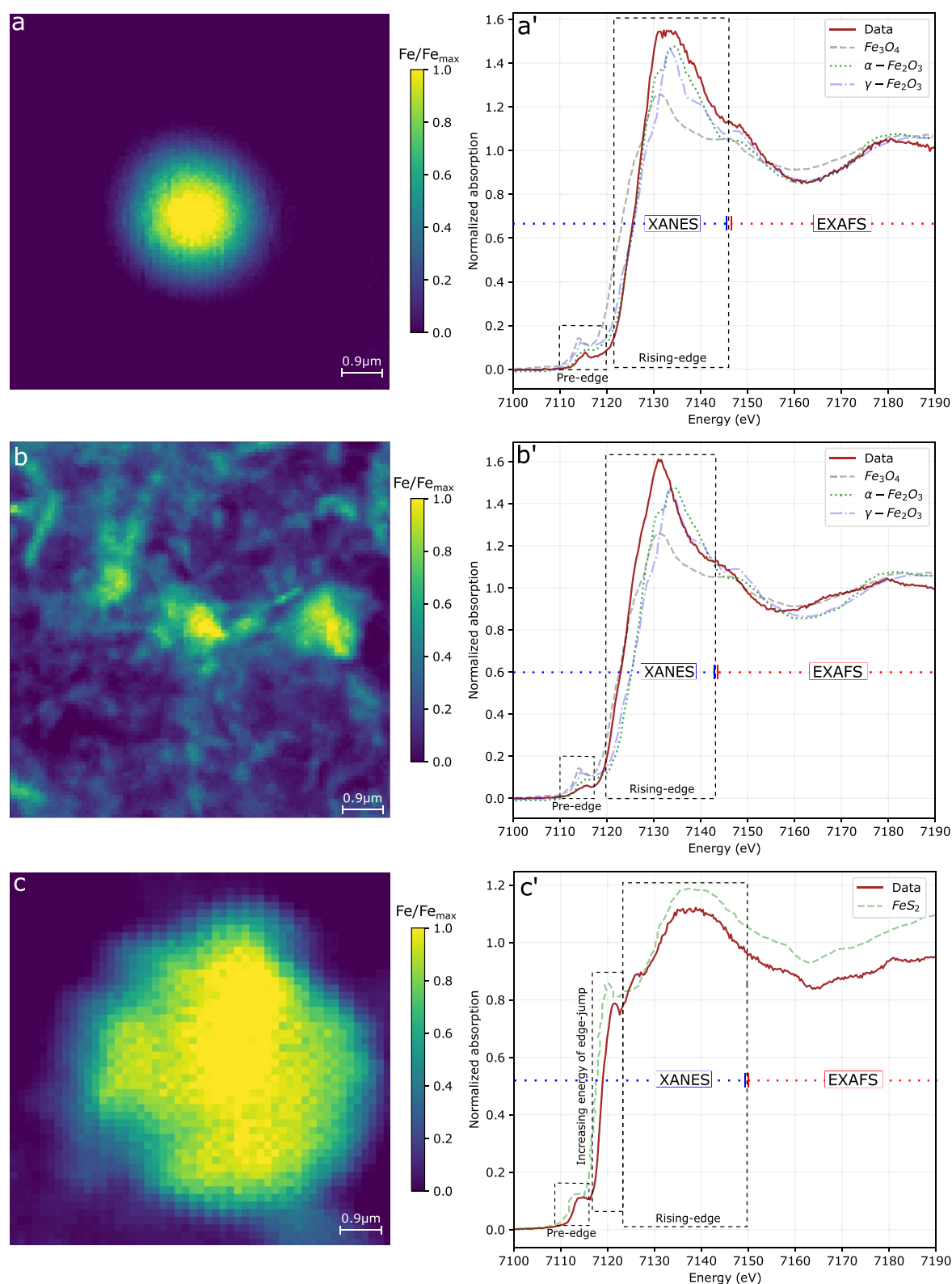


Figure 9. Compositional maps of Fe (K α \approx 6400 eV) for the Sete-Lagoas, Salitre, and Guia samples (a–c, respectively). Normalized XAS spectrum collected in fluorescence mode around the iron activation energy ($E_0 \approx$ 7112 eV) are shown in the right column (a'–c'), and compared to data extracted from literature: for magnetite (Fe_3O_4), maghemite ($\gamma\text{-Fe}_2\text{O}_3$), and hematite ($\alpha\text{-Fe}_2\text{O}_3$) from Piquer et al. (2014); and pyrite (FeS_2) from Ravel (2013).

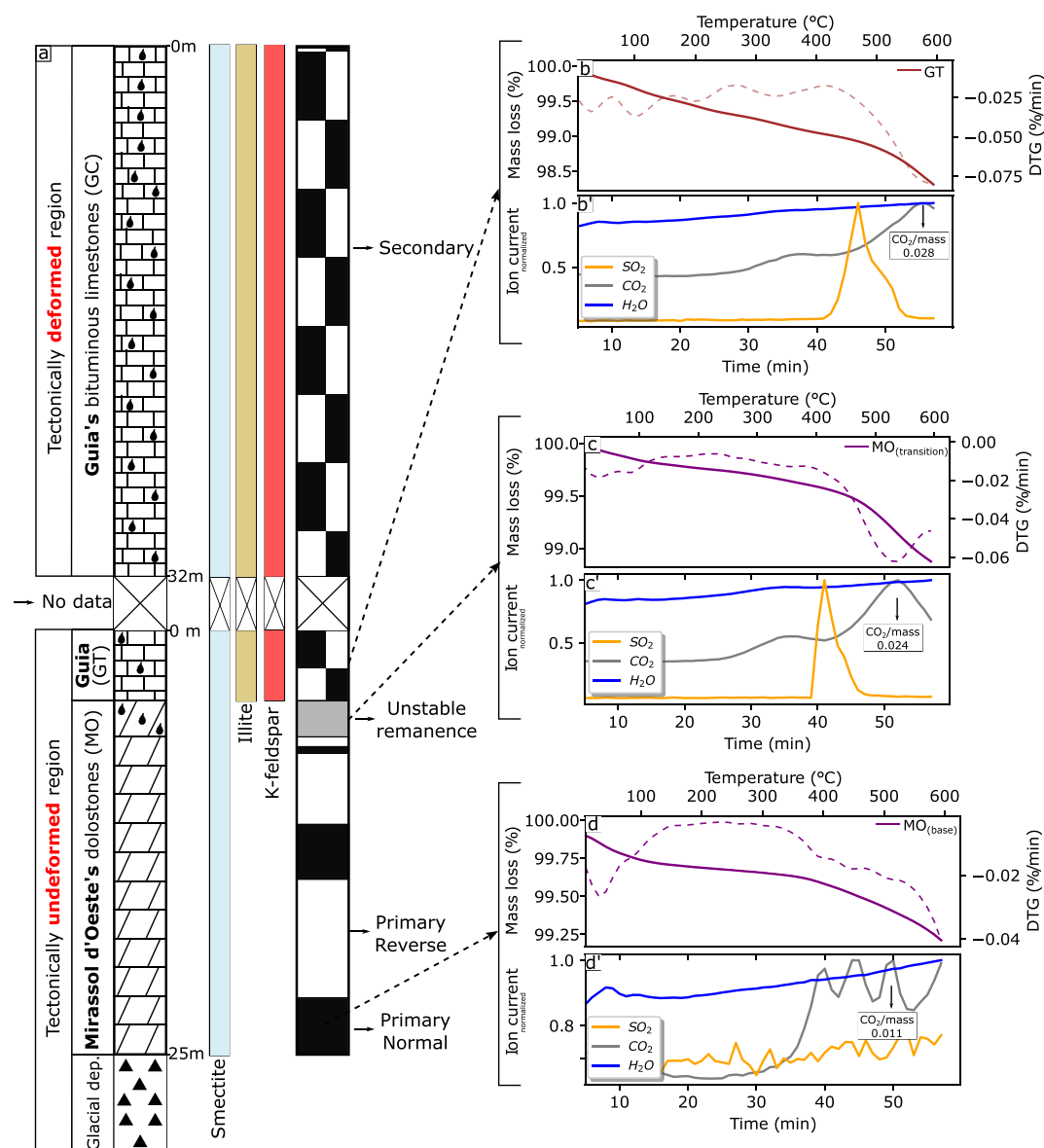


Figure 10. (a) Stratigraphic profiles of the Araras Group over the deformed (Paraguay belt) and undeformed regions (Amazon craton), modified from Trindade et al. (2003) and Font et al. (2006). Blue, ocher, and red bars indicate where the presence of smectite, illite, and K-feldspar (respectively). These minerals were detected through either XRD, petrography, or SEM analysis. The polarity chart, modified from Font et al. (2010), shows that the Guia Formation only yields a remagnetized component, while percolation of bitumen in the upper section of the Mirassol d'Oeste formation ($MO_{transition}$) has completely erased stable remanence. In the right column, thermogravimetric analysis coupled to a Quadrupole Mass Spectrometer (TGA-QMS) shows the mass loss (%) of the basal stratum of (b) Mirassol d'Oeste (MO_{base}), its bitumen-enriched portion (c) ($MO_{transition}$) and the overlying (d) Guia Formation (GT). Normalized ion current flow (b'–d') allows the detection the volatilized emissions throughout the heating process.

while dolomite decomposition occurs between 700°C and 750°C (Gunasekaran & Anbalagan, 2007); therefore, the CO₂ loss we observe is unrelated carbonate decomposition. The observed CO₂ liberation is, however, typical for bitumen decomposition, with peak liberation at 550°C (Zhao et al., 2012). Importantly, TGA-QMS analysis reveals that bitumen is also present at the base of the Mirassol d'Oeste formation (MO_{base}), corroborating previous findings (Júnior et al., 2016). However, when examining the ion current normalized by the individual mass of the samples (CO₂/mass at the CO₂'s major peak), the Mirassol d'Oeste samples at the contact with the Guia formation ($MO_{transition}$), as well as GT samples, contain twice the mass of bitumen compared to MO_{base} . This

confirms that bitumen percolation was less effective at the base of the Mirassol d'Oeste formation, likely contributing to the preservation of detrital remanence.

SO₃ emissions were not detected in the TGA-QMS analysis, but SO₂ emissions were detectable in the GT and MO_{transition} samples (Figures 10b' and 10c'). For GT samples, SO₂ emissions occur between 420°C and 540°C, while for MO_{transition} samples, they occur between approximately 400°C–430°C. These emissions are interpreted as related to pyrite, as we discuss ahead.

In atmospheres with high O₂ concentrations at temperatures <800 K, pyrite will directly oxidize, but in low O₂ atmospheres (or at higher temperatures), it will first oxidize to a mineral of the troilite group (Hu et al., 2006). Between 400°C and 600°C in atmospheric air, pyrite decomposes to form FeS and S, with S further combining with oxygen to form SO₂, and FeS sequentially reacting with oxygen gas to form iron sulfate (Zunino & Scrivener, 2022). TGA analysis performed on pyrite-bearing shales reports SO₂ emissions between 400°C and 430°C (Labus, 2020) (as in our samples). The grain size of pyrite particles also influences the range of SO₂ emissions because thermal decomposition strongly influences kinetic phenomena. Emissions from fine particles (<45 µm) begin around 320°C and stop around 540°C, while emissions from larger particles (<200 µm) begin around 450°C and stop around 550°C (Zumaquero et al., 2021). Pyrrhotite decomposition in GT samples is likely contained within the higher temperature SO₂ emissions, but as these are too restricted in MO_{transition} samples, they probably fall outside the detection range.

5. Discussion

5.1. Remagnetization Fingerprints (?) of South American Neoproterozoic Carbonates

Distortions in hysteresis, IRM, and ARM curves are common in natural samples due to the mix of grains with varying magnetic properties (Egli, 2003; Tauxe et al., 1996). These distortions are often analyzed using unmixing techniques to better understand the characteristics of different components. Grain populations may differ due to variations in composition or domain states. During geological events that trigger the growth of new magnetic grains, some grains may grow beyond their blocking volume, stabilizing their magnetic state, while others remain below the superparamagnetic (SP) threshold and cannot sustain magnetic recording. This explains the significant presence of SP particles in remagnetized carbonates, highlighting the importance of accurately identifying and quantifying SP particles within the grain population.

Superparamagnetic (SP) particles significantly influence magnetic hysteresis (Tauxe et al., 1996) and susceptibility at both low and high frequencies (Hrouda et al., 2013), yet accurately quantifying them remains challenging. The presence of distinct coercivity components can also lead to potbelly and wasp-waisted hysteresis profiles (Tauxe et al., 1996). In remagnetized carbonates, multiple mineral alteration pathways can produce sufficient quantities of various magnetic minerals, impacting the overall magnetic properties of samples. While our data, as seen in the Day plot (Figure 3), do not align perfectly with the typical “remagnetized fingerprint,” they consistently exhibit properties characteristic of the PSD (pseudo-single-domain) state.

The PSD state acts as a transition between the SD (single-domain) and MD (multi-domain) states, encompassing a range of magnetic domain configurations, from single to multi-vortex states, which often feature magnetization helicity. While SD grains are known for their long-term magnetic stability (Butler, 1992), recent studies performed by Nagy et al. (2017) using micromagnetic models have identified an unstable magnetic zone (UMZ) where grain sizes approach 50% of the SD range. In this zone, domain configurations like hard-aligned SV (HSV) and easy-aligned SV (ESV) emerge. Although ESV structures can offer magnetic stability surpassing that of SD grains (Nagy et al., 2019b), HSV configurations typically remain unstable even at room temperature (Nagy et al., 2017). The size range for this UMZ in equidimensional octahedral grains of magnetite is 84–100 nm, although this varies with the mineralogy and morphology (Nagy et al., 2019b; Wang et al., 2022).

Particles within the unstable magnetic zone (UMZ) exhibit not only decreased thermal stability but also altered magnetic properties such as reduced coercivity and increased susceptibility, similar to superparamagnetic (SP) particles (Nagy et al., 2019b; Wang et al., 2022). These changes in the UMZ can complicate the interpretation of magnetic data from remagnetized carbonates, as the distorted hysteresis loops and frequency-dependent susceptibility might be mistakenly attributed to the presence of SP grains. Authigenic growth processes and chemical alterations like maghemitization might push fine-grained particles into the UMZ, impacting their magnetic stability, as possibly seen in the Bambuí sample (Figure 9b).

FORC diagrams provide a more accurate method for identifying magnetic domain states in samples with multiple magnetic minerals. In our studies, remagnetized carbonates show FORC diagrams with a central ridge indicative of non-interacting single domain/PSD grains (Roberts et al., 2022), corroborated by direct microscopic observations (Figures 8 and 9). Despite the evidence for the presence of SP grains, their contribution to the rock's overall magnetic properties remains debatable, especially given the limitations of frequency-dependent susceptibility in distinguishing these features.

As shown, typical hysteresis and backfield curves of remagnetized rocks may exhibit very similar characteristics to those of rocks bearing primary remanence, which can pose challenges in recognizing remagnetization effects. However, integrating magnetic analyses with high-resolution chemical and mineralogical studies can enhance our understanding of remagnetization mechanisms and their geological implications in sedimentary environments.

5.2. West Gondwana Large Scale Remagnetization

5.2.1. Mechanisms for Authigenic Mineral Formation

Understanding the primary cause of remagnetization in rocks remains challenging, despite using a multidisciplinary approach. The responsible process must be extensive enough to affect large areas, such as entire intracratonic basins. Fluid percolation is a plausible mechanism but requires the carbonate sequences to have uniform porosity and permeability to facilitate widespread remagnetization quickly. While orogenic fluid percolation could be influential, the similar mineralogical composition of these basins suggests that mineral transformation, particularly from smectite to illite, might be a critical factor. Additionally, the geotectonic context, including the final amalgamation of Gondwana and the Brasiliano orogenies, must also be considered in understanding the remagnetization events (Figure 1a).

Our interpretation focuses on the diagenetic evolution of sedimentary basins and assesses the implications of various phenomena on the growth and preservation of remanence. K-feldspars, detected in all remagnetized units through XRD or petrographic observations, coexist with smectite and illite. The influx of terrigenous materials into cap carbonates, likely driven by glacial melting, introduces significant K^+ into the pore waters. Early diagenetic reactions mobilize sulfur ions, leading to the formation of mackinawite, a precursor to other iron sulfides (Rickard, 1995). As temperatures rise, conditions in the sedimentary basin stabilize to a more reducing environment with slightly acidic to basic pH levels. This promotes the consumption of metastable iron-hydroxides by iron-reducing bacteria, preserving only the most stable iron oxides. The presence of S^{2-} , from mackinawite consumption, and available Fe^{2+} encourage pyrite nucleation, hindered kinetically under such conditions (Rickard & Luther, 2007). Smectite-illitization initiates around 70°C (Huggett, 2005), releasing more Fe^{2+} ions, favorable for authigenic magnetite growth and chemical stability (Pourbaix, 1974). With increasing pressure and depth, reaching up to 120°C, magnetite particles gradually acquire a chemical remanent magnetization during the illitization peak.

The studied rocks, showing signs of compaction, incipient chloritization, and specific illite crystallinity indices indicative of epizone temperatures, likely reached the low greenschist facies (around 300°C). As conditions transition from diagenesis to incipient metamorphism (anchizone) at higher temperatures, magnetite continues to grow. However, beyond 180°C, the growth of monoclinic pyrrhotite becomes kinetically (Lennie et al., 1995) and thermodynamically (Ning et al., 2015) favored, potentially under similar pH/Eh conditions favorable for magnetite. Sequentially, the thermodynamic stability of pyrite may collapse due to limited sulfur and iron, potentially leading to its dissolution and providing the necessary ions for the growth of monoclinic pyrrhotite and further magnetite, thereby contributing to the acquisition of a chemical remanent magnetization (Brothers et al., 1996).

Aubourg et al. (2019) explored the occurrence of magnetite and monoclinic pyrrhotite in clay-rich rocks, specifically shales and slates. The primary objective was to discern the coexistence patterns of these minerals under different temperature conditions, utilizing magnetic remanence analysis. Their findings indicated that magnetite and SP-pyrrhotite were simultaneously present within the temperature range of 77°C–128°C. Additionally, at temperatures ranging from 300°C to 350°C, MD magnetite coexisted with SD pyrrhotite, while temperatures exceeding 347°C exclusively revealed the presence of pyrrhotite. The study suggests that the formation of pyrrhotite may occur at the expense of magnetite and can function as a temperature indicator. It also proposes that rocks of this nature, when subjected to metamorphic conditions, would record the magnetic field due to

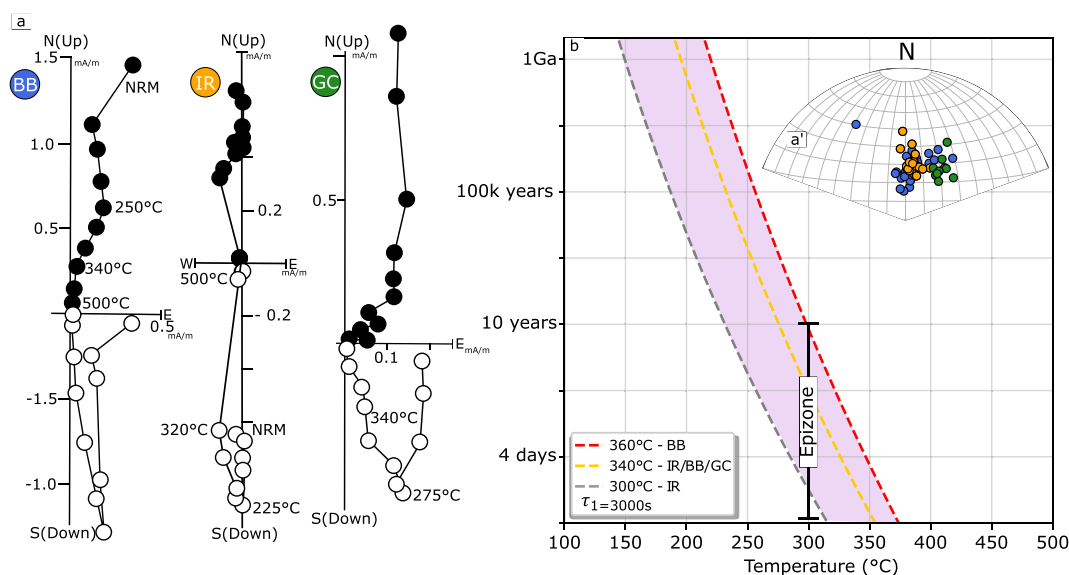


Figure 11. Coherence in thermal demagnetization behavior of different samples of Neoproterozoic carbonates in South America. (a) Zijderveld diagrams of thermally demagnetized samples from the Sete Lagoas Formation (BB), from D'Agrella-Filho et al. (2000); Salitre Formation (IR), from Trindade et al. (2004); and Guia Formation in the Cáceres region (GC), from Font et al. (2006). (a') Blue, orange, and green circles represent site mean directions of the BB, IR, and GC units (respectively). (b) Pullaiah's nomogram (Pullaiah et al., 1975) for magnetite, illustrating that the viscous relaxation curves (calculated using the blocking temperatures marked with dashed lines) suggest that these remanences could be easily unblocked over a short period when exposed to epizone conditions. The lower boundary of the epizone is where relaxation curves intersect the 300°C isotherm. τ_1 represents the laboratory heating time.

subsequent denudation processes and cooling down, essentially exhibiting a thermoremanent magnetization (TRM). However, our samples presented some distinctive characteristics. Petrographic observation and the illite crystallinity index both indicated incipient metamorphic conditions extending well beyond 128°C but limited to low greenschist. Furthermore, the paleomagnetic components obtained from the thermal demagnetization of the Sete Lagoas, Salitre, and Guia formations (Figure 11a) displayed unique demagnetization behaviors attributed to both PSD/SD monoclinic pyrrhotite and magnetite, resulting in almost indistinguishable directions (Figure 11a').

Because the detrital sources in the carbonate matrix are not homogeneously distributed, different sectors of a macro/micro-region can be influenced by the influx of Fe^{2+} or S^{2-} (from smectite-illitization and/or sulfide dissolution) and therefore favor the growth of either one of these ferrimagnetic minerals. Therefore, the remanence of authigenically grown phases could completely overcome a DRM or pDRM in terms of intensity (Kars et al., 2012), explaining why only a secondary component is observed in the carbonates of the Sete Lagoas and Salitre formations.

5.2.2. A Syn-Collisional or a Post-Collisional Secondary Remanence?

Although the formation of authigenic ferromagnetic grains in these Neoproterozoic carbonates and their characteristic remanence is likely influenced by the continental collisions that took place during the Late Neoproterozoic/Early Cambrian, their remanence is most likely not from such a period. In other words, although a product of a process that leads to a g-CRM, a thermal effect is effectively unblocking/blocking the remanence. To interpret the timing of the remanence, three key points must be considered: (a) the single polarity observed in the data; (b) the constrained, low-dispersed paleomagnetic directions; and (c) the paleomagnetic position of the poles in relation to the Gondwana APW curve. Firstly, the temperature issue is addressed, explaining why these samples are believed to have been thermally remagnetized.

Paleotemperature data derived from the illite crystallinity index (KI) align with previous thermal demagnetization studies (D'Agrella-Filho et al., 2000; Trindade et al., 2004; Font et al., 2006). For example, magnetite in the samples shows lower-range blocking temperatures of 340–360°C for Sete Lagoas (BB) samples, 300–340°C for Salitre (IR) samples, and 300°C for GC samples (Figure 11a). These temperatures correspond with medium-to-

high inclination vectors with an NNE trend (Figure 11a'), supported by their paleomagnetic pole positions (Figure 1b).

Assuming the lower boundary of the epizone environment (300°C) as the peak temperature for these rocks, and following Néel's theory (Néel, 1955), it is posited that grains initially carrying a g-CRM could lose their remanence when heated to an unblocking temperature T_1 over a relaxation time τ_1 . This corresponds to a geological time τ_2 at a temperature T_2 (Pullaiah et al., 1975). Using Pullaiah's approach, viscous relaxation curves (Figure 11b) demonstrate that exposure to 300°C for a short period (<10 years) would be sufficient to completely relax their remanence. In a continental setting where basins remain under low greenschist metamorphic conditions, remanence would continually reset until a decrease in temperature occurs. In such context, an original g-CRM component carried by monoclinic pyrrhotite, statistically similar to that of magnetite, would be easily erased in epizone conditions since their blocking temperatures do not surpass 300°C.

In this scenario, a cooling event is necessary to lock their remanence. Similar to magnetite, pyrrhotite's viscous decay becomes steeper near its Curie temperature (Dunlop et al., 2000). Since none of the samples from the Bambuí, Irecê, or Araras regions exhibited blocking temperatures below 250°C (D'Agrella-Filho et al., 2000; Font et al., 2006; Trindade et al., 2004), the blocking of directions during environmental heat dissipation, even at slow cooling rates, would occur rapidly. There is a subtle difference in the characteristic remanence between pyrrhotite and magnetite components in these rocks. The former yields mean site directions with a lower precision parameter (k) and larger confidence ellipses (α_{95}) than the latter. This could be explained by sequential cooling and blocking of each of these phases being chronologically slightly separated, with magnetite blocking first, followed by pyrrhotite.

The paleomagnetic record of pyrrhotite-bearing rocks, exposed to metamorphic conditions, can effectively register the magnetic field as they cool (Rochette et al., 1992). The sequence of thermomagnetic experiments conducted by Crouzet et al. (2001) on multipolarity-bearing remagnetized carbonates of the Western Alps confirms that single-domain pyrrhotite can sequentially register pTRMs (post-thermal remanent magnetizations) during slow cooling. Unlike remagnetized rocks bearing multipolarity components, samples from Bambuí, Irecê, and Guia exhibit only a single polarity component related to pyrrhotite/magnetite. While tectonic collisions likely raised temperatures, facilitating reactions that formed authigenic magnetic minerals (as explained in the previous section), if the remanence would represent this period (i.e., would be slowly acquired through burial diagenesis), we would expect to see a dual-polarity remanence. The reason is that during the Late Ediacaran-Early Cambrian, the Earth's magnetic field exhibited intense activity, with extremely low field strength ($<2 \cdot 10^{22} \text{ A}^2\text{m}^2$, Bono et al. (2019)) and high reversal rates, sometimes reaching 20 reversals per million years (20 R/Myr, Levashova et al. (2021)). The absence of dual polarity in a progressively buried sample recording remanence over such a chaotic period would be improbable. A thermoviscous overprint, caused by a heating event followed by cooling, could explain the contemporaneity of these components and the large-scale remagnetization event affecting Gondwana.

The most likely causes for the elevation of temperatures to low greenschist metamorphic conditions are the collision events of the Brasiliano (Panafrican) orogenies. These orogenies, which occurred during the Late Precambrian—Early Paleozoic, led to the amalgamation of various terranes with the Amazon and São Francisco Cratons (Almeida et al., 1973; Mohriak & Fainstein, 2012). The closure of the Clymene Ocean and the bending of the Paraguay belt (located between the southeastern margin of the Amazon craton and the São Francisco Craton, Figure 2b) reached peak metamorphic conditions around $528 \pm 36 \text{ Ma}$ ($^{40}\text{Ar}/^{39}\text{Ar}$) (Tohver et al., 2010). Such events could have remagnetized parts of the Guia Formation over the Cáceres region (GC, Paraguay Belt) and provided a diffusion heat source for nearby areas, where this formation is less affected over the Amazon Craton (GT), as shown by smaller Kübler Index values.

For the São Francisco Craton, the Araçuaí belt along its eastern border (Figure 2a) has a long magmatic history spanning from 630 to 480 Ma Tedeschi et al. (2016) and Pedrosa-Soares (2020), with metamorphic peaks around 580 Ma (Pedrosa-soares et al., 2007). The cooling history of the Araçuaí Belt may account for a regional heat dissipation that originated the epizone conditions indicated by the illite-crystallinity calculations in both the Bambuí and Irecê areas. This hypothesis is supported by previous studies that have reported greenschist metamorphism in carbonates from the Bambuí (Caby & Costa Campos Neto, 2022; Misi et al., 2014), including the presence of metamorphic chlorite.

Furthermore, the observation that these geologically distinct units, separated by hundreds of kilometers, exhibit statistically indistinguishable paleomagnetic directions suggests not only simultaneous heating but also a tightly constrained cooling period. Early 2000 s paleomagnetic studies by Trindade et al. (2004) and D'Agregella-Filho et al. (2000) positioned the paleomagnetic poles of these remagnetized rocks around the 520 Ma interval on the Gondwana APW curve. However, when aligned with the mean paleomagnetic poles APW curve of Gondwana (Torsvik et al., 2012) (Figure 1b), the directions align more closely with the 460–470 Ma interval. Notably, the high-quality poles from West Gondwana, such as the SAVN (Araçuaí orogen in Brazil, 500 Ma) and CF (Pampia terrane in Argentina, 519 Ma), differ significantly from those of the remagnetized carbonates (Table 1).

The blocking of remanent magnetization in these carbonates is likely linked to the Early- to Middle-Ordovician period. The Late Cambrian/Early Paleozoic marks the end of Gondwana's assembly and the orogenic collapse of Neoproterozoic belts, including the Araçuaí-Ribeira along the Brazilian Atlantic coast (Alkmim et al., 2006; Pedrosa-Soares et al., 2001; Wiedemann et al., 2002) and the Damara orogen in Southwest Africa (Goscombe et al., 2018). This period is characterized by significant post-collisional magmatism, and the cessation of main orogenic activities likely resulted in the relaxation of upwardly compressed isotherms (Fonseca et al., 2021). A Paleozoic cooling event is evident across much of West Gondwana, with the earliest zircon AHe and ZHe ages from the Neoproterozoic Dom Feliciano belt in South Brazil ranging from 472 to 26 Ma. The Ordovician ages suggest an exhumation of the crystalline basement. Similarly, apatite fission track ages in the Brasília belt show a rapid cooling around 480 Ma, indicating basement exhumation (Fonseca et al., 2020). Early Paleozoic cooling ages in the São Francisco Craton escalate toward the Devonian, likely influenced by interplate tectonic readjustments and erosional processes, potentially enhanced by Late Ordovician glaciation Torsvik and Cocks (2013).

If the remanence observed in these units is indeed associated with this Paleozoic cooling event, it could provide an explanation for the single polarity directions observed for magnetite/pyrrhotite in these carbonates across such a large continental area. During this period, the Amazon and São Francisco cratons would have been in the southern hemisphere (Merdith et al., 2021), potentially linking these components to the Moyero superchron (Pavlov & Gallet, 2005).

5.3. Hydrocarbon Percolation in Carbonates of the Araras Group

Even if we consider the secondary remanence of carbonates from the Guia Formation as preserved from the Paleozoic cooling event in both deformed (GC) and undeformed (GT) terrains, some important questions about the Araras Group carbonates emerge, such as: What role does hydrocarbon percolation play? And why did only the limestones in the Guia Formation undergo remagnetization, while the bitumen-enriched upper section of Mirassol d'Oeste did not?

Considering the first question, the alteration of hydrocarbon to bitumen in the Guia Formation likely occurred in situ (indigenous origin) (Júnior et al., 2016). This process certainly influenced local thermochemical equilibrium and the generation/destruction of magnetic phases. Hydrocarbon biodegradation is also important for ion exchange within the pore water and it depends on various environmental factors such as oxygen, nitrogen, phosphorus, carbon availability, salinity, pressure, rock permeability, porosity, pH levels, and temperature. These factors are essential for the development of bacterial colonies, which could influence the formation of authigenic magnetic minerals (Banerjee et al., 1997; Fruit et al., 1995). Moreover, the processes of smectite illitization and organic matter maturation may overlap, especially in clays with high organic matter, facilitating interactions that enhance the production of magnetic minerals (Elmore et al., 2012; Kennedy et al., 2002).

To suggest an answer to the second question, we consider the remanence carriers and the mineralogical composition of the rocks from the Araras Group. Font et al. (2005) describe the primary remanence of Mirassol d'Oeste dolostones as held by specular hematite and magnetite. In turn, the Guia Formation over the Paraguay belt shows remanence held by both monoclinic pyrrhotite and magnetite, while the undeformed region over the Amazon craton is dominated by pyrrhotite only (Font et al., 2006). However, our results have shown that even if stable remanence is not carried by magnetite in GT samples, this mineral is still present in these rocks.

Our TGA-QMS provides insights into organic matter percolation within Araras Group samples by correlating the release of volatile phases, particularly CO₂ and SO₂, with increasing temperature. This corresponds to the decomposition of bitumen and pyrite. We observe a significant presence of bitumen in the upper portion of the Mirassol d'Oeste formation ($MO_{transition}$), where stable remanence disappears (see Figure 10a). It's likely that

hydrogen sulfide, commonly found in petroleum (Shi & Wu, 2021), contributes to the dissolution of iron oxides/hydroxides and sulfides, causing the loss of primary remanence in the upper section of the Mirassol d'Oeste formation, as hydrocarbon percolation is less prominent at the base of these cap carbonates (see emission in Figure 10d') (Font et al., 2006).

If biodegradation/maturation of hydrocarbons were the sole factor responsible for generating authigenic magnetic minerals in the Guia Formation, we would expect to observe stable remanence during the transition from Mirassol d'Oeste to the Guia Formation, similar to what is observed in GT samples. Our assessment of Illite crystallinity indicates that rocks from the Guia Formation over the Amazon craton exhibit slightly higher *KI* values compared to those over the Paraguay belt, suggesting temperatures within the anchizone range (70–120°C). These temperatures are sufficient for the transformation of smectite to illite, suggesting that clay transformation may have been crucial for the growth of stable remanence carriers in the Terconi quarry. However, no significant sources of K^+ , essential for illitization, were detected in samples from Mirassol d'Oeste through petrographic or XRD analyses (Huggett, 2005). This absence of potassium sources likely inhibits the authigenesis of pyrrhotite and magnetite in MO samples. Since the original detrital magnetic phases of the upper section of the Mirassol d'Oeste would not have withstood the hydrocarbon maturation processes, no stable remanence is observed.

Besides, the higher temperatures in the Paraguay belt, which favor multiple geochemical processes including clay transformation and organic matter maturation, should have potentially led to a greater volume of magnetite particles in the Cáceres region compared to the Terconi quarry. This probably led to more magnetite particles achieving blocking volumes and recording stable remanence alongside pyrrhotite.

Lastly, the compositional differences between the Guia Formation and the base of the Mirassol d'Oeste Formation—interpreted by us as critical in determining whether remagnetization occurred—add further confidence that the magnetization held by the cap carbonates at the base of the Araras Group is indeed primary. Most paleomagnetic experiments did not show a clear distinction between the magnetic properties of the primary remanence carriers and those that were remagnetized (e.g., the magnetic hysteresis parameters in Figure 3). However, FORC diagrams suggest a more significant contribution of non-interacting SD/PSD grains in the matrix of remagnetized carbonate samples (see Figure 4) compared to those of the Mirassol d'Oeste Formation. We interpret this as evidence for the growth of authigenic phases. This additional evidence supporting the primary origin of the remanence in the cap dolostones is a key contribution, as their presence has important implications for Snowball Earth models (Font et al., 2005; Trindade et al., 2003).

6. Conclusion

In this manuscript, we have investigated the remagnetization of Neoproterozoic carbonate rocks from South America, specifically the rocks from the Araras Group (Amazon Craton) and the Sete Lagoas and Salitre Formations (São Francisco Craton). We have employed rock magnetic analyses alongside macro/microchemical and imaging approaches. In this context, we scrutinize not only the extensive remagnetization influencing intra-cratonic basins throughout West Gondwana, elucidating the geological phenomena underpinning it but also appraise how the magnetic characteristics of these carbonates do not necessarily align with anticipated magnetic “fingerprints” associated with carbonate remagnetization.

Except for samples from the Irecê Basin, the hysteresis parameters in our study deviated from the globally observed cluster of remagnetized rocks. Instead, they closely align with non-remagnetized carbonate units around the pseudo-single domain area. This discrepancy leads to a “false negative” scenario for the identified fingerprint. The unusual Bcr/Bc ratios in remagnetized carbonates typically correspond to mixtures of SD + SP particles. Despite our efforts to quantify the SP contribution through susceptibility loss in frequency-dependent measurements, which indicated a susceptibility loss of over 5% in most samples from remagnetized units, we cannot solely attribute this behavior to SP particles due to the limitations of the method. Additionally, samples from our control unit, the base of the Mirassol d'Oeste (non-remagnetized), show a susceptibility loss comparable to that of the Bambuí (Sete-Lagoas Formation) and Irecê (Salitre Formation), highlighting another challenge to the original fingerprint assumptions.

On the other hand, FORC diagrams reveal a predominant distribution along the coercivity axis, indicating a broad spectrum of non-interacting single-domain/pseudo-single-domain grains. For instance, FORC distributions frequently reach zero coercivities, potentially providing more concrete evidence of SP particles in these rocks. In

contrast, the non-remagnetized unit demonstrates a much larger contribution to the interaction axis rather than the coercivity axis.

Regarding the processes that remagnetized these rocks, while fluid percolation can indeed induce changes in the redox/pH state of the environment and prompt alterations, these changes would likely be localized along the pathways of fluid percolation if the rocks lack uniform porosity/permeability. However, we propose that the development of secondary magnetic minerals is intricately linked to temperature increases and the smectite-illite transformation, which releases Fe^{2+} into the medium. The released iron can then nucleate to generate magnetite and/or react with sulfur from the dissolution of other sulfides (e.g., pyrite), leading to the generation of monoclinic pyrrhotite as temperatures rise. XRD analysis, supported by petrographic/microscopic data, confirms the presence of both smectite and highly crystalline illite, along with mineral sources of K^+ (orthoclase) necessary for the reaction to occur. In all the examined samples, we observe a spatial correlation of aluminosilicates with iron oxides/sulfides through micro-XRF. Significantly, XAS analysis allows us to confirm the presence of irregularly shaped grains of pure magnetite and core-shell structures of maghemite-magnetite within the aluminosilicates, both with the matching dimensions of the PSD threshold. Specifically in the Guia formation (where bitumen is abundant), the generation of these authigenic phases is believed to be an interplay between organic matter maturation/biodegradation and smectite-illitization.

Henceforth, we recommend that researchers investigating carbonate sedimentary systems with high detrital content from a paleomagnetic standpoint should examine both the presence and composition of clay minerals. Additionally, they should explore the spatial relationship between these clay minerals and potential carriers of remanence, as clay transformation may play a significant constraint on magnetic mineral authigenesis.

Our discussion explores processes closely linked to the initial formation of minerals below their respective Curie temperatures, ultimately leading to the acquisition of chemical remanent magnetization. However, our proposition suggests that the current remanence observed in these Neoproterozoic carbonates is a result of thermoremanent magnetization. A key observation supporting this interpretation is the statistically similar single-polarity directions exhibited by both pyrrhotite and magnetite components across all these basins. This suggests a rapid blocking process capable of influencing a vast continental area. Analysis of the thermal demagnetization data from these samples leads us to infer that only a few thousand years of exposure to temperatures above 300°C would suffice to thermally relax the magnetization of both pyrrhotite and magnetite. The crystalline index of illite in these samples, combined with petrographic observations and previous data, confirms that these samples likely experienced temperatures equivalent to low-greenschist grades. We propose that such heat was generated during the final amalgamation of Gondwana. As heat propagation gradually increases, it unblocks the remanence of these ferrimagnetic phases, prompting a constant reset of the remanence. In conclusion, sequential cooling after the Brasiliano orogeny relaxes the isotherms previously shifted upwards due to the collision. Consequently, this process blocks the remanences in these basins across the continent. These remanences reflect poles falling close to the Early Middle Ordovician medium poles of the Gondwana apparent polar wander path.

Data Availability Statement

The experimental data reported in this research is stored at Zenodo (Bellon, Williams, et al., 2023) and can be publicly accessed at <https://doi.org/10.5281/zenodo.10283417>.

References

- Aldana, M., Costanzo-Alvarez, V., Gomez, L., Gonzalez, C., Diaz, M., Silva, P., & Rada, M. (2011). Identification of magnetic minerals related to hydrocarbon authigenesis in Venezuelan oil fields using an alternative decomposition of isothermal remanence curves. *Studia Geophysica et Geodaetica*, 55(2), 343–358. <https://doi.org/10.1007/s11200-011-0019-0>
- Alkmim, F., Marshak, S., Pedrosa-Soares, A., Peres, G., Cruz, S., & Whittington, A. (2006). Kinematic evolution of the Araçuaí-West Congo Orogen in Brazil and Africa: Nutcracker tectonics during the neoproterozoic assembly of Gondwana. *Precambrian Research*, 149(1–2), 43–64. <https://doi.org/10.1016/j.precamres.2006.06.007>
- Almeida, F., Amaral, G., Cordani, U., & Kawashita, K. (1973). The Precambrian evolution of the South America cratonic margin south of the Amazon River. In *The ocean basins and margins* (pp. 411–446). Plenum Publishing.
- Alvarenga, C. (1990). *Phénomènes sédimentaires, structuraux et circulation de fluides développés à la transition chaïrcir;ne-craton. exemple de la chaîne paraguay d'âge protérozoïque supérieur, mato grosso, Brésil*. Aix-Marseille University III.
- Alvarenga, C., & Trompette, R. (1992). Glacially influenced sedimentation in the Later Proterozoic of the Paraguay belt (Mato Grosso, Brazil). *Palaeogeography, Palaeoclimatology, Palaeoecology*, 92(1–2), 85–105. [https://doi.org/10.1016/0031-0182\(92\)90136-S](https://doi.org/10.1016/0031-0182(92)90136-S)

Acknowledgments

Magnetic experiments were performed at the USPMag lab at the Instituto de Astronomia, Geofísica e Ciências Atmosféricas (IAG) of the Universidade de São Paulo (USP). X-ray diffraction data were collected at the Institute of Energy and Environment (IEE) of the University of São Paulo. Special recognition to Dra. Cilene de Medeiros and Dra. Ingrid Barcelos, for the assistance provided when collecting SEM-EDS data at the Microscopic Sample Laboratory, at the Brazilian Synchrotron Light Laboratory (LNLS). Experiments performed at the CARNAUBA beamline (LNLS) are related to proposal 20220316. This work is funded by the São Paulo Research Foundation (FAPESP), Grants 21/00861-2, 22/14100-6, and 16/06114-6. The opinions, hypotheses, and conclusions or recommendations expressed in this material are the responsibility of the authors and do not necessarily reflect the views of FAPESP. W.W. would like to acknowledge support from the Natural Environmental Research Council through Grants NE/V001233/1 and NE/S011978/1. Lastly, we extend our gratitude to Mark Dekkers, Agnes Kontny, Eric Font, and an anonymous reviewer, whose reviews and criticism greatly helped to improve this paper.

- Aubourg, C., Jackson, M., Ducoux, M., & Mansour, M. (2019). Magnetite-out and pyrrhotite-in temperatures in shales and slates. *Terra Nova*, 31(6), 534–539. <https://doi.org/10.1111/ter.12424>
- Babinski, M., Liu, D., Trindade, R. I. F., & Brito Neves, B. B. (2004). U-pb shrimp ages of detrital zircons from bebedouro formation, northeast Brazil: Constraints on sediment provenance and depositional age of Neoproterozoic glacial rocks of the São Francisco Craton. In *Abstracts. IUGS*. Retrieved from <https://repositorio.usp.br/directbitstream/c5bb5309-d34d-440d-b7e2-8314e28a0ff4/1393157.pdf>
- Babinski, M., Vieira, L., & Trindade, R. (2007). Direct dating of the Sete Lagoas cap carbonate (Bambu Group, Brazil) and implications for the Neoproterozoic glacial events. *Terra Nova*, 19(6), 401–406. <https://doi.org/10.1111/j.1365-3121.2007.00764.x>
- Bachtadse, V., Voo, R., & Hällich, I. (1987). Paleomagnetism of the western Cape Fold Belt, South Africa, and its bearing on the paleozoic apparent polar wander path for Gondwana. *Earth and Planetary Science Letters*, 84(4), 487–499. [https://doi.org/10.1016/0012-821X\(87\)90013-6](https://doi.org/10.1016/0012-821X(87)90013-6)
- Banerjee, S., Elmore, R. D., & Engel, M. H. (1997). Chemical remagnetization and burial diagenesis: Testing the hypothesis in the Pennsylvanian Belden Formation, Colorado. *Journal of Geophysical Research*, 102(B11), 24825–24842. <https://doi.org/10.1029/97JB01893>
- Bellon, U. D., Trindade, R., & Williams, W. (2023). Unmixing of magnetic hysteresis loops through a modified Gamma-Cauchy exponential model. *Geochemistry, Geophysics, Geosystems*, 24(8), 1–21. <https://doi.org/10.1029/2023GC011048>
- Bellon, U. D., Williams, W., Trindade, R., Galante, D., Sant'Anna, L. G., & Pescarini, T. (2023). Magnetic properties and chemical analysis of remagnetised carbonates of South America [Dataset]. *Zenodo*. <https://doi.org/10.5281/zenodo.10283417>
- Bono, R. K., Tarduno, J. A., Nimmo, F., & Cottrell, R. D. (2019). Young inner core inferred from Ediacaran ultra-low geomagnetic field intensity. *Nature Geoscience*, 12(2), 143–147. <https://doi.org/10.1038/s41561-018-0288-0>
- Brothers, L., Engel, M., & Elmore, R. (1996). The late diagenetic conversion of pyrite to magnetite by organically complexed ferric iron. *Chemical Geology*, 130(1), 1–14. [https://doi.org/10.1016/0009-2541\(96\)00007-1](https://doi.org/10.1016/0009-2541(96)00007-1)
- Butler, R. (1992). *Paleomagnetism: Magnetic domains to geologic terranes*. Blackwell Scientific Publications. Retrieved from https://books.google.com.br/books?id=q_NzQgAACAAJ
- Butler, R., & Banerjee, S. (1975). Theoretical single-domain grain size range in magnetite and titanomagnetite. *Journal of Geophysical Research*, 80(29), 4049–4058. <https://doi.org/10.1029/jb080i029p04049>
- Caby, R., & Costa Campos Neto, M. (2022). Basement domes in a greenschist facies context: Tectono-metamorphic evolution of the southern Quadrilátero Ferrífero, southeast Brazil. *Tectonophysics*, 828, 229280. <https://doi.org/10.1016/j.tecto.2022.229280>
- Carvallo, C., Muxworthy, A., & Dunlop, D. (2006). First-order reversal curve (FORC) diagrams of magnetic mixtures: Micromagnetic models and measurements. *Physics of the Earth and Planetary Interiors*, 154(3–4), 308–322. <https://doi.org/10.1016/j.pepi.2005.06.017>
- Carvallo, C., Özdemir, O., & Dunlop, D. (2004). First-order reversal curve (FORC) diagrams of elongated single-domain grains at high and low temperatures. *Journal of Geophysical Research: Solid Earth*, 109(4). <https://doi.org/10.1029/2003JB002539>
- Chemale, J., Alkmin, F., & Endo, I. (1993). Late proterozoic tectonism in the interior of the São Francisco Craton. In H. Dispersal (Ed.), *Gondwana eight—Assembly evolution* (pp. 29–42). Balkema.
- Couto, D. (2020). Mineralogy composition and texture indicative of fluid-assisted remobilization in carbonate units of the Irecê Basin, Brazil. *Journal of South American Earth Sciences*, 110, 103346. <https://doi.org/10.1016/j.jsames.2021.103346>
- Crouzet, C., Rochette, P., & Ménard, G. (2001). Experimental evaluation of thermal recording of successive polarities during uplift of meta-sediments. *Geophysical Journal International*, 145(3), 771–785. <https://doi.org/10.1046/j.0956-540x.2001.01423.x>
- D'Agrella-Filho, M. (1995). Paleomagnetism of carbonatic sedimentary sequences of the Salitre Formation, Chapada Diamantina—Bahia. In *4th International Congress of the Brazilian Geophysical Society* (pp. 262–265). Sociedade Brasileira de Geofísica.
- D'Agrella-Filho, M., Babinski, M., Trindade, R., Schmus, W., & Ernesto, M. (2000). Simultaneous remagnetization and u–pb isotope resetting in neoproterozoic carbonates of the São Francisco Craton, Brazil. *Precambrian Research*, 99(3–4), 179–196. [https://doi.org/10.1016/S0301-9268\(99\)00059-5](https://doi.org/10.1016/S0301-9268(99)00059-5)
- D'Agrella-Filho, M., Irene, M., Raposo, B., & Egydio-silva, M. (2004). Paleomagnetic study of the Juiz de Fora complex, SE Brazil: Implications for Gondwana. *Gondwana Research*, 7(1), 103–113. [https://doi.org/10.1016/s1342-937x\(05\)70309-9](https://doi.org/10.1016/s1342-937x(05)70309-9)
- D'Agrella-Filho, M., & Pacca, I. (1986). Paleomagnetism of metamorphic rocks from the piquete region-ribeira valley, southeastern Brazil. *Revista Brasileira de Geociências*, 4, 79–84.
- Dannemann, S., Appel, E., Rösler, W., Neumann, U., Liebke, U., & Nag, D. (2022). Palaeomagnetic indication for India–Asia collision at 12°N and maximum 810 km greater India extent in the western suture zone. *Geophysical Journal International*, 229(2), 1193–1211. <https://doi.org/10.1093/gji/ggab528>
- Dardenne, M., & Freitas-Silva, M. (1998). Depósitos pb–zn–f–ba do supergrupo São Francisco. In *Proceedings of the XI congresso brasileiro de geologia, 1998*. Belo Horizonte, Minas Gerais.
- Davidson, M., Egger, J., Elmore, R., Engel, M., Woods, S., & Abraham, M. (2000). Orogenic fluids and secondary magnetizations: Testing the relationship in the South Wales Coalfield foreland basin. *Journal of Geochemical Exploration*, 70, 581–584. [https://doi.org/10.1016/s0375-6742\(00\)00063-7](https://doi.org/10.1016/s0375-6742(00)00063-7)
- Day, R., Fuller, M., & Schmidt, V. (1977). Hysteresis properties of titanomagnetites: Grain-size and compositional dependence. *Physics of the Earth and Planetary Interiors*, 13(4), 260–267. [https://doi.org/10.1016/0031-9201\(77\)90108-X](https://doi.org/10.1016/0031-9201(77)90108-X)
- Dearing, J., Dann, R. J. L., Hay, K., Lees, J. A., Loveland, P. J., Maher, B. A., & O'Grady, K. (1996). Frequency-dependent susceptibility measurements of environmental materials. *Geophysical Journal International*, 124(1), 228–240. <https://doi.org/10.1111/j.1365-246X.1996.tb06366.x>
- Duncan, D. (2018). Synchrotron-based spectroscopy in on-surface polymerization of covalent networks. In *Encyclopedia of interfacial chemistry, Surface science and electrochemistry* (pp. 436–445). Elsevier.
- Dunlop, D. (2002). Theory and application of the day plot (mrs/ms versus hcr/hc) 1. Theoretical curves and tests using titanomagnetite data. *Journal of Geophysical Research*, 107(B3). <https://doi.org/10.1029/2001JB000486>
- Dunlop, D., & Özdemir, O. (1997). *Rock magnetism: Fundamentals and frontiers* (1st ed.). Cambridge University Press.
- Dunlop, D., Özdemir, O., Clark, D., & Schmidt, P. (2000). Time–temperature relations for the remagnetization of pyrrhotite (Fe₇S₈) and their use in estimating paleotemperatures. *Earth and Planetary Science Letters*, 176(1), 107–116. [https://doi.org/10.1016/S0012-821X\(99\)00309-X](https://doi.org/10.1016/S0012-821X(99)00309-X)
- Egli, R. (2003). Analysis of the field dependence of remanent magnetization curves. *Journal of Geophysical Research: Solid Earth*, 108(B2), 1–25. <https://doi.org/10.1029/2002jb002023>
- Egli, R. (2013). Variforc: An optimized protocol for calculating non-regular first-order reversal curve (FORC) diagrams. *Global and Planetary Change*, 110, 302–320. <https://doi.org/10.1016/j.gloplacha.2013.08.003>
- Egli, R., Chen, A., Winklhofer, M., Kodama, K., & Horng, C.-S. (2010). Detection of noninteracting single domain particles using first-order reversal curve diagrams. *Geochemistry, Geophysics, Geosystems*, 11(1). <https://doi.org/10.1029/2009GC002916>

- Elmore, R. D., Muxworthy, A. R., & Aldana, M. (2012). Remagnetization and chemical alteration of sedimentary rocks. *Geological Society of London*, 371, 1–21. <https://doi.org/10.1144/sp371.15>
- Emmertson, S., Muxworthy, A., Sephton, M., Aldana, M., Costanzo-Alvarez, V., Bayona, G., & Williams, W. (2013). Correlating biodegradation to magnetization in oil bearing sedimentary rocks. *Geochimica et Cosmochimica Acta*, 112, 146–165. <https://doi.org/10.1016/j.gca.2013.03.008>
- Figueiredo, F., Almeida, R., Tohver, E., Babinski, M., Liu, D., & Fanning, C. (2009). Neoproterozoic glacial dynamics revealed by provenance of diamictites of the bebedouro formation, São Francisco Craton, central eastern Brazil. *Terra Nova*, 21(5), 375–385. <https://doi.org/10.1111/j.1365-3121.2009.00893.x>
- Fonseca, A., Novo, T., Nachtergaele, S., Fonte-Boa, T., Ranst, G., & Grave, J. (2021). Differential phanerozoic evolution of cratonic and non-cratonic lithosphere from a thermochronological perspective: São Francisco craton and marginal orogens (Brazil). *Gondwana Research*, 93, 106–126. <https://doi.org/10.1016/j.gr.2021.01.006>
- Fonseca, A., Piffer, G., Nachtergaele, S., Ranst, G., Grave, J., & Novo, T. (2020). Devonian to permian post-orogenic denudation of the Brasília belt of west Gondwana: Insights from apatite fission track thermochronology. *Journal of Geodynamics*, 137, 101733. <https://doi.org/10.1016/j.jog.2020.101733>
- Font, E., Nédélec, A., Trindade, R., & Moreau, C. (2010). Fast or slow melting of the marinoan snowball Earth? The cap dolostone record. *Palaeogeography, Palaeoclimatology, Palaeoecology*, 295(1), 215–225. <https://doi.org/10.1016/j.palaeo.2010.05.039>
- Font, E., Rapalini, A. E., Tomezzoli, R. N., Trindade, R. I. F., & Tohver, E. (2012). Episodic remagnetizations related to tectonic events and their consequences for the South America polar wander path. *Geological Society, London, Special Publications*, 371(1), 55–87. <https://doi.org/10.1144/SP371.7>
- Font, E., Trindade, R., & Nédélec, A. (2005). Detrital remanent magnetization in haematite-bearing Neoproterozoic Puga cap dolostone, Amazon craton: A rock magnetic and SEM study. *Geophysical Journal International*, 163(2), 491–500. <https://doi.org/10.1111/j.1365-246X.2005.02776.x>
- Font, E., Trindade, R., & Nédélec, A. (2006). Remagnetization in bituminous limestones of the neoproterozoic araras group (Amazon craton): Hydrocarbon maturation, burial diagenesis, or both? *Journal of Geophysical Research: Solid Earth*, 111(6), 1–17. <https://doi.org/10.1029/2005JB004106>
- Franceschini, P., Rapalini, A., Escayola, M., & Picada, C. (2019). Paleogeographic and tectonic evolution of the pampia terrane in the Cambrian: New paleomagnetic constraints. *Tectonophysics*, 779, 228386. <https://doi.org/10.1016/j.tecto.2020.228386>
- Fruit, D., Elmore, R. D., & Halgedahl, S. (1995). Remagnetization of the folded belden formation, northwest Colorado. *Journal of Geophysical Research*, 100(B8), 15009–15023. <https://doi.org/10.1029/95JB00045>
- Gaucher, C., Boggiani, P., Sprechmann, P., Sial, A., & Fairchild, T. (2003). Integrated correlation of the Vendian to Cambrian Arroyo del Soldado and Corumbá Groups (Uruguay and Brazil): Palaeogeographic, palaeoclimatic and palaeobiologic implications. *Precambrian Research*, 120(3–4), 241–278. [https://doi.org/10.1016/S0301-9268\(02\)00140-7](https://doi.org/10.1016/S0301-9268(02)00140-7)
- Geiss, C., Egli, R., & Zanner, C. (2008). Direct estimates of pedogenic magnetite as a tool to reconstruct past climates from buried soils. *Journal of Geophysical Research*, 113(B11), 11102. <https://doi.org/10.1029/2008JB005669>
- Golovanova, I. V., Danukalov, K. N., Salmanova, R. Y., Levashova, N. M., Parfiriev, N. P., Sergeeva, N. D., & Meert, J. G. (2023). Magnetic field hyperactivity during the early Neoproterozoic: A paleomagnetic and cyclostratigraphic study of the Katav Formation, southern Urals, Russia. *Geoscience Frontiers*, 14(4), 101558. <https://doi.org/10.1016/j.gsf.2023.101558>
- Goscombe, B., Foster, D., Gray, D., & Wade, B. (2018). The evolution of the damara orogenic system: A record of west Gondwana assembly and crustal response. In S. Siegesmund, M. A. Basei, P. Oyhantçabal, & S. Oriolo (Eds.), *Geology of Southwest Gondwana* (pp. 303–352). Springer.
- Grotzinger, J. P., & James, N. P. (2000). Precambrian carbonates: Evolution of understanding. In J. P. Grotzinger & N. P. James (Eds.), *Carbonate sedimentation and diagenesis in the evolving Precambrian world* (pp. 3–20). Society for Sedimentary Geology.
- Guacaneme, C., Babinski, M., Paula-Santos, G., & Pedrosa-Soares, A. (2017). C, O, and sr isotopic variations in Neoproterozoic-Cambrian carbonate rocks from sete lagoas formation (Bambuí Group), in the southern São Francisco Basin, Brazil. *Brazilian Journal of Geology*, 47(3), 521–543. <https://doi.org/10.1590/2317-4889201720160126>
- Guimarães, G., Pierosan, R., & Ruiz, A. (2017). Geologia e petrologia do Granito São Vicente na região do Parque Estadual Águas Quentes, estado de Mato Grosso, Brasil. *Geologia USP: Série Científica*, 17(3), 29. <https://doi.org/10.11606/issn.2316-9095.v17-426>
- Gunasekaran, S., & Anbalagan, G. (2007). Thermal decomposition of natural dolomite. *Bulletin of Materials Science*, 30(4), 339–344. <https://doi.org/10.1007/s12034-007-0056-z>
- Harrison, R., Muraszko, J., Heslop, D., Lascu, I., Muxworthy, A., & Roberts, A. (2018). An improved algorithm for unmixing first-order reversal curve diagrams using principal component analysis. *Geochemistry, Geophysics, Geosystems*, 19(5), 1595–1610. <https://doi.org/10.1029/2018gc007511>
- Heslop, D., Roberts, A. P., Oda, H., Zhao, X., Harrison, R. J., Muxworthy, A. R., et al. (2020). An automatic model selection-based machine learning framework to estimate forc distributions. *Journal of Geophysical Research: Solid Earth*, 125(10), 1–16. <https://doi.org/10.1029/2020JB020418>
- Hirt, A. M., Banin, A., & Gehring, A. U. (1993). Thermal generation of ferromagnetic minerals from iron-enriched smectites. *Geophysical Journal International*, 115(3), 1161–1168. <https://doi.org/10.1111/j.1365-246X.1993.tb01518.x>
- Hrouda, F. (2011). Models of frequency-dependent susceptibility of rocks and soils revisited and broadened. *Geophysical Journal International*, 187(3), 1259–1269. <https://doi.org/10.1111/j.1365-246X.2011.05227.x>
- Hrouda, F., Pokorný, J., Ježek, J., & Chadima, M. (2013). Out-of-phase magnetic susceptibility of rocks and soils: A rapid tool for magnetic granulometry. *Geophysical Journal International*, 194(1), 170–181. <https://doi.org/10.1093/gji/ggt097>
- Hu, G., Dam-Johansen, K., Wedel, S., & Hansen, J. (2006). Decomposition and oxidation of pyrite. *Progress in Energy and Combustion Science*, 32(3), 295–314. <https://doi.org/10.1016/j.peccs.2005.11.004>
- Huang, W., Lippert, P., Jackson, M., Dekkers, M., Zhang, Y., Li, J., et al. (2017). Remagnetization of the Paleogene Tibetan Himalayan carbonate rocks in the Gamba area: Implications for reconstructing the lower plate in the India-Asia collision. *Journal of Geophysical Research: Solid Earth*, 122(2), 808–825. <https://doi.org/10.1002/2016JB013662>
- Huggett, J. M. (2005). Sedimentary rocks—Clays and their diagenesis. In *Encyclopedia of geology* (pp. 62–70). Elsevier. <https://doi.org/10.1016/B0-12-369396-9/00311-7>
- Jaboyedoff, M., Bussy, F., Kübler, B., & Thelin, P. (2001). Illite “crystallinity” revisited. *Clays and Clay Minerals*, 49(2), 156–167. <https://doi.org/10.1346/CCMN.2001.0490205>
- Jackson, M. (1990). Diagenetic sources of stable remanence in remagnetized Paleozoic cratonic carbonates: A rock magnetic study. *Journal of Geophysical Research*, 95(B3), 2753–2761. <https://doi.org/10.1029/JB095iB03p02753>

- Jackson, M., & Swanson-Hysell, N. (2012). Rock magnetism of remagnetized carbonate rocks: Another look. *Geological Society - Special Publications*, 371(1), 229–251. <https://doi.org/10.1144/SP371.3>
- Jiao, W., Li, Y., Yang, Z., & Liu, J. (2019). A widespread early mesozoic remagnetization in South China. *Journal of Geophysical Research: Solid Earth*, 124(1), 88–103. <https://doi.org/10.1029/2018JB016707>
- Júnior, G., Nogueira, A., Neto, E., Moura, C., Araújo, B., & Reis, F. (2016). Organic matter in the neoproterozoic cap carbonate from the Amazonian craton, Brazil. *Journal of South American Earth Sciences*, 72, 7–24. <https://doi.org/10.1016/j.jsames.2016.07.012>
- Kars, M., Aubourg, C., Pozzi, J., & Janots, D. (2012). Continuous production of nanosized magnetite through low grade burial. *Geochemistry, Geophysics, Geosystems*, 13(8). <https://doi.org/10.1029/2012GC004104>
- Karunadasa, K., Manoratne, C., Pitawala, H., & Rajapakse, R. (2019). Thermal decomposition of calcium carbonate (calcite polymorph) as examined by in-situ high-temperature x-ray powder diffraction. *Journal of Physics and Chemistry of Solids*, 134, 21–28. <https://doi.org/10.1016/j.jpcs.2019.05.023>
- Kennedy, M. J., Pevear, D. R., & Hill, R. J. (2002). Mineral surface control of organic carbon in black shale. *Science*, 295(5555), 657–660. <https://doi.org/10.1126/science.1066611>
- Kübler, B. (1964). Les argiles indicateurs de métamorphisme. In *Revue de l'Institut Français du Pétrole* (Vol. 29, pp. 1096–1113).
- Kübler, B. (1967). La cristallinité de l'illite et les zones tout à fait supérieures du métamorphisme. In *Etages tectoniques, colloque de neuchâtel* (pp. 105–121).
- Kübler, B. (1968). Evaluation quantitative du métamorphisme par cristallinité de l'illite. *Bull Centre Rech Pau-SNPA*, 2, 385–397.
- Kübler, B. (1990). "Cristallinité" de l'illite et mixed-layer: Brève révision. *Schweizerische Mineral. Petrographische Mitteilungen*, 70, 89–93.
- Labus, M. (2020). Pyrite thermal decomposition in source rocks. *Fuel*, 287, 119529. <https://doi.org/10.1016/j.fuel.2020.119529>
- Lanson, B., Sakharov, B. A., Claret, F., & Drits, V. A. (2009). Diagenetic smectite-to-illite transition in clay-rich sediments: A reappraisal of x-ray diffraction results using the multi-specimen method. *American Journal of Science*, 309(6), 476–516. <https://doi.org/10.2475/06.2009.03>
- Lascu, I., Einsle, J., Ball, M., & Harrison, R. (2018). The vortex state in geologic materials: A micromagnetic perspective. *Journal of Geophysical Research: Solid Earth*, 123(9), 7285–7304. <https://doi.org/10.1029/2018JB015909>
- Lennie, A., England, K., & Vaughan, D. (1995). Transformation of synthetic mackinawite to hexagonal pyrrhotite; a kinetic study. *American Mineralogist*, 80(9–10), 960–967. <https://doi.org/10.2138/am-1995-9-1012>
- Levashova, N. M., Golovanova, I. V., Rudko, D., Danukalov, K. N., Rudko, S., Yu, S. R., & Meert, J. G. (2021). Late ediacaran magnetic field hyperactivity: Quantifying the reversal frequency in the Zigan Formation, southern Urals, Russia. *Gondwana Research*, 94, 133–142. <https://doi.org/10.1016/j.gr.2021.02.018>
- Levi, S. (2007). Magnetization, chemical remanent (CRM). In D. Gubbins & E. Herrero-Bervera (Eds.), *Encyclopedia of geomagnetism and paleomagnetism* (pp. 580–588). Springer. https://doi.org/10.1007/978-1-4020-4423-6_190
- Lowrie, W. (1990). Identification of ferromagnetic minerals in a rock by coercivity and unblocking temperature properties. *Geophysical Research Letters*, 17(2), 159–162. <https://doi.org/10.1029/GL017i002p00159>
- Machel, H. (2001). Bacterial and thermochemical sulfate reduction in diagenetic settings—Old and new insights. *Sedimentary Geology*, 140(1–2), 143–175. [https://doi.org/10.1016/S0037-0738\(00\)00176-7](https://doi.org/10.1016/S0037-0738(00)00176-7)
- Mählmann, R., & Frey, M. (2012). Standardisation, calibration and correlation of the Kübler-index and the vitrinite/bituminite reflectance: An inter-laboratory and field related study. *Swiss Journal of Geosciences*, 105(2), 153–170. <https://doi.org/10.1007/s00015-012-0110-8>
- Matamoras-Veloza, A., Cespedes, O., Johnson, B. R. G., Stawski, T. M., Terranova, U., de Leeuw, N. H., & Benning, L. G. (2018). A highly reactive precursor in the iron sulfide system. *Nature Communications*, 9(1), 3125. <https://doi.org/10.1038/s41467-018-05493-x>
- McCabe, C., & Elmore, R. (1989). The occurrence and origin of late paleozoic remagnetization in the sedimentary rocks of north America. *Reviews of Geophysics*, 27(4), 471–494. <https://doi.org/10.1029/RG027i004p00471>
- McCabe, C., Voo, R., Peacor, D., Scotese, C., & Freeman, R. (1983). Diagenetic magnetite carries ancient yet secondary remanence in some paleozoic sedimentary carbonates. *Geology*, 11(4), 221–223. [https://doi.org/10.1130/0091-7613\(1983\)11](https://doi.org/10.1130/0091-7613(1983)11)
- Merdith, A. S., Williams, S. E., Collins, A. S., Tetley, M. G., Mulder, J. A., Blades, M. L., et al. (2021). Extending full-plate tectonic models into deep time: Linking the Neoproterozoic and the Phanerozoic. *Earth-Science Reviews*, 214, 103477. <https://doi.org/10.1016/j.earscirev.2020.103477>
- Miller, J., & Kent, D. (1988). Regional trends in the timing of Alleghanian remagnetization in the Appalachians. *Geology*, 16(7), 588–591. [https://doi.org/10.1130/0091-7613\(1988\)016<0588:rtitto>2.3.co;2](https://doi.org/10.1130/0091-7613(1988)016<0588:rtitto>2.3.co;2)
- Misi, A., Azmy, K., Kaufman, A., Oliveira, T., Sanches, A., & Oliveira, G. (2014). Review of the geological and geochronological framework of the Vazante sequence, Minas Gerais, Brazil: Implications to metallogenic and phosphogenic models. *Ore Geology Reviews*, 63, 76–90. <https://doi.org/10.1016/j.oregeorev.2014.05.002>
- Misi, A., & Kyle, J. (1994). Upper proterozoic carbonate stratigraphy, diagenesis, and stromatolitic phosphorite formation, Irecê Basin, Bahia, Brazil. *Journal of Sedimentary Research*, 64A(2), 299–310. <https://doi.org/10.1306/d4267d84-2b26-11d7-8648000102c1865d>
- Misi, A., & Veizer, J. (1998). Neoproterozoic carbonate sequences of the Una Group, Irecê Basin, Brazil: Chemostratigraphy, age and correlations. *Precambrian Research*, 89(1–2), 87–100. [https://doi.org/10.1016/S0301-9268\(97\)00073-9](https://doi.org/10.1016/S0301-9268(97)00073-9)
- Mohriak, W., & Fainstein, R. (2012). Phanerozoic regional geology of the eastern Brazilian margin. In *Regional geology and tectonics: Phanerozoic passive margins, cratonic basins and global tectonic maps* (pp. 222–282). Elsevier.
- Moreira, D., Uhlein, A., Dussin, I., Uhlein, G., & Misuzaki, A. (2020). A Cambrian age for the upper Bambuí Group, Brazil, supported by the first u-pb dating of volcanoclastic bed. *Journal of South American Earth Sciences*, 99, 102503. <https://doi.org/10.1016/j.jsames.2020.102503>
- Muxworthy, A., & Dunlop, D. (2002). First-order reversal curve (FORC) diagrams for pseudo-single-domain magnetites at high temperature. *Earth and Planetary Science Letters*, 203(1), 369–382. [https://doi.org/10.1016/S0012-821X\(02\)00880-4](https://doi.org/10.1016/S0012-821X(02)00880-4)
- Nagy, L., Williams, W., Muxworthy, A. R., Fabian, K., Almeida, T. P., Conbhuí, P. Ó., & Shcherbakov, V. P. (2017). Stability of equidimensional pseudo-single-domain magnetite over billion-year timescales. *Proceedings of the National Academy of Sciences of the United States of America*, 114(39), 10356–10360. <https://doi.org/10.1073/pnas.1708344114>
- Nagy, L., Williams, W., Tauxe, L., & Muxworthy, A. R. (2019a). From nano to micro: Evolution of magnetic domain structures in multidomain magnetite. *Geochemistry, Geophysics, Geosystems*, 20(6), 2907–2918. <https://doi.org/10.1029/2019GC008319>
- Nagy, L., Williams, W., Tauxe, L., Muxworthy, I., & Ferreira, A. (2019b). Thermomagnetic recording fidelity of nanometer-sized iron and implications for planetary magnetism. *Proceedings of the National Academy of Sciences of the United States of America*, 116(6), 1984–1991. <https://doi.org/10.1073/pnas.1810797116>
- Néel, L. (1955). Some theoretical aspects of rock-magnetism. *Advances in Physics*, 4(14), 191–243. <https://doi.org/10.1080/00018735500101204>
- Ning, J., Zheng, Y., Brown, B., Young, D., & Nesic, S. (2015). Construction and verification of pourbaix diagrams for hydrogen sulfide corrosion of mild steel. In *NACE - International Corrosion Conference Series* (pp. 1–19).

- Nogueira, A., & Riccomini, C. (2006). O Grupo Araras (Neoproterozóico) na parte norte da Faixa Paraguai e sul do Craton Amazônico, Brasil. *Revista Brasileira de Geociências*, 36(4), 576–587. <https://doi.org/10.25249/0375-7536.2006364576587>
- Nogueira, A., Riccomini, C., Sial, A., Moura, C., & Fairchild, T. (2003). Soft-sediment deformation at the base of the Neoproterozoic Puga cap carbonate (southwestern Amazon Craton, Brazil): Confirmation of rapid icehouse to greenhouse transition in snowball Earth. *Geology*, 31(7), 613–616. [https://doi.org/10.1130/0091-7613\(2003\)031](https://doi.org/10.1130/0091-7613(2003)031)
- Oliveira, L., Gonçalves, M., & Tella, V. (2014). Projeto Sirius: A nova fonte de luz síncrotron brasileira.
- Oliver, J. (1986). Fluids expelled tectonically from orogenic belts: Their role in hydrocarbon migration and other geologic phenomena. *Geology*, 14(2), 99–102. [https://doi.org/10.1130/0091-7613\(1986\)14<99:FETFOB>2.0.CO;2](https://doi.org/10.1130/0091-7613(1986)14<99:FETFOB>2.0.CO;2)
- Parry, L. (1982). Magnetization of immobilized particle dispersions with two distinct particle sizes. *Physics of the Earth and Planetary Interiors*, 28(3), 230–241. [https://doi.org/10.1016/0031-9201\(82\)90004-8](https://doi.org/10.1016/0031-9201(82)90004-8)
- Patarachao, B. (2019). Xrd analysis of illite-smectite interstratification in clays from oil sands ores. *Advances in X-Ray Analysis*, 62(C), 22–31.
- Paula-Santos, G., Babinski, M., Kuchenbecker, M., Caetano-Filho, S., Trindade, R., & Pedrosa-Soares, A. (2015). New evidence of an Ediacaran age for the Bambuí Group in southern São Francisco Craton (eastern Brazil) from zircon u–pb data and isotope chemostratigraphy. *Gondwana Research*, 28(2), 702–720. <https://doi.org/10.1016/j.gr.2014.07.012>
- Pavlov, V., & Gallet, Y. (2005). A third superchron during the early paleozoic. *International Union of Geological Sciences*, 28(2), 78–84. <https://doi.org/10.18814/epiuiugs/2005/v28i2/001>
- Pedrosa-Soares, A. (2020). O Orógeno Araçuaí à luz da Geocronologia: Um tributo a Umberto Cordani. In A. November, W. Teixeira, & B. Neves (Eds.), *Geocronologia e Evolução Tectônica do Continente Sul-Americano: A Contribuição de Umberto Giuseppe Cordani* (1st ed., pp. 250–272). Solaris Edições Culturais.
- Pedrosa-Soares, A., Noce, C., Wiedemann, C., & Pinto, C. (2001). The Araçuaí-west-Congo orogen in Brazil: An overview of a confined orogen formed during Gondwanaland assembly. *Precambrian Research*, 110(1–4), 307–323. [https://doi.org/10.1016/S0301-9268\(01\)00174-7](https://doi.org/10.1016/S0301-9268(01)00174-7)
- Pedrosa-soares, A., Noce, C. M., Alkmim, F. F., Silva, L. C., Babinski, M., Cordani, U., & Castañeda, C. (2007). Orógeno Araçuaí: Síntese do conhecimento 30 anos após almeida 1977. *Geonomos*, 15(1), 1–16. <https://doi.org/10.18285/geonomos.v15i1.103>
- Penner-Hahn, J. (2003). X-ray absorption spectroscopy. In *Comprehensive coordination chemistry* (Vol. 2, pp. 159–186). Elsevier. <https://doi.org/10.1016/b0-08-043748-6/01063-x>
- Piceda, C., Franceschini, P., Escayola, M., & Rapalini, A. (2018). Paleomagnetism of the Santa Victoria Group in the Mojotoro Range, Salta: Contributions to the paleogeographic position of Pampia in early Paleozoic [paleomagnetismo del grupo santa victoria en la sierra de mojotoro, salta: Aportes a la reconstrucción pal]. *Revista de la Asociacion Geologica Argentina*, 75(4), 518–532. Retrieved from <https://revista.geologica.org.ar/raga/article/view/134>
- Pike, C., Roberts, A., Dekkers, M., & Verosub, K. (2001). An investigation of multi-domain hysteresis mechanisms using forc diagrams. *Physics of the Earth and Planetary Interiors*, 126(1–2), 11–25. [https://doi.org/10.1016/S0031-9201\(01\)00241-2](https://doi.org/10.1016/S0031-9201(01)00241-2)
- Piquer, C., Laguna-Marco, M., Roca, A., Boada, R., Guglieri, C., & Chaboy, J. (2014). Fe k-edge x-ray absorption spectroscopy study of nanosized nominal magnetite. *Journal of Physical Chemistry*, 118(2), 1332–1346. <https://doi.org/10.1021/jp4104992>
- Pourbaix, M. (1974). *Atlas of electrochemical equilibria in aqueous solutions* (1st ed., Vol. 2, p. 1). National Association of Corrosion Engineers.
- Pullaiah, G., Irving, E., Buchan, K., & Dunlop, D. (1975). Magnetization changes caused by burial and uplift. *Earth and Planetary Science Letters*, 28(1), 133–143. <https://doi.org/10.1177/001139217502300101>
- Rapalini, A. E., & Bettucci, L. S. (2008). Widespread remagnetization of late Proterozoic sedimentary units of Uruguay and the apparent polar wander path for the Rio de La Plata craton. *Geophysical Journal International*, 174(1), 55–74. <https://doi.org/10.1111/j.1365-246X.2008.03771.x>
- Rapalini, A. E., Trindade, R. I., & Poiré, D. G. (2013). The la tinta pole revisited: Paleomagnetism of the Neoproterozoic Sierras Bayas Group (Argentina) and its implications for Gondwana and Rodinia. *Precambrian Research*, 224, 51–70. <https://doi.org/10.1016/j.precamres.2012.09.007>
- Ravel, B. (2013). Xas-education, examples, FES2. In *Transmission scan of FES2*. Retrieved from https://github.com/bruceravel/XAS-Education/blob/06b144d1a3418c3f1ddec2454167d62f58f1f256/Examples/FeS2/fes2_rt01_mar02.xmu
- Ravel, B., & Newville, M. (2005). Athena, artemis, hephaestus: Data analysis for x-ray absorption spectroscopy using ifeffit. *Journal of Synchrotron Radiation*, 12(4), 537–541. <https://doi.org/10.1107/S0909049505012719>
- Riccomini, C., Nogueira, A., & Sial, A. (2007). Carbon and oxygen isotope geochemistry of ediacaran outer platform carbonates, Paraguay belt, central Brazil. *Anais Da Academia Brasileira De Ciências*, 79(3), 519–527. <https://doi.org/10.1590/s0001-37652007000300012>
- Rickard, D. (1995). Kinetics of FES precipitation: Part 1. Competing reaction mechanisms. *Geochimica et Cosmochimica Acta*, 59(21), 4367–4379. [https://doi.org/10.1016/0016-7037\(95\)00251-T](https://doi.org/10.1016/0016-7037(95)00251-T)
- Rickard, D., & Luther, G. (2007). Chemistry of iron sulfides. *Chemical Reviews*, 107(2), 514–562. <https://doi.org/10.1021/cr0503658>
- Roberts, A. (2015). Magnetic mineral diagenesis. *Earth-Science Reviews*, 151, 1–47. <https://doi.org/10.1016/j.earscirev.2015.09.010>
- Roberts, A., Florindo, F., Villa, G., Chang, L., Jovane, L., Bohaty, S. M., et al. (2011). Magnetotactic bacterial abundance in pelagic marine environments is limited by organic carbon flux and availability of dissolved iron. *Earth and Planetary Science Letters*, 310(3–4), 441–452. <https://doi.org/10.1016/j.epsl.2011.08.011>
- Roberts, A., Heslop, D., Zhao, X., Oda, H., Egli, R., Harrison, R. J., et al. (2022). Unlocking information about fine magnetic particle assemblages from first-order reversal curve diagrams: Recent advances. *Earth-Science Reviews*, 227, 103950. <https://doi.org/10.1016/j.earscirev.2022.103950>
- Roberts, A., Heslop, D., Zhao, X., & Pike, C. (2014). Understanding fine magnetic particle systems through use of first-order reversal curve diagrams. *Reviews of Geophysics*, 52(4), 557–602. <https://doi.org/10.1002/2014RG000462>
- Roberts, A., Pike, C., & Verosub, K. (2000). First-order reversal curve diagrams: A new tool for characterizing the magnetic properties of natural samples. *Journal of Geophysical Research: Solid Earth*, 105(B12), 28461–28475. <https://doi.org/10.1029/2000jb900326>
- Rochette, P., Ménard, G., & Dunn, R. (1992). Thermochronometry and cooling rates deduced from single sample records of successive magnetic polarities during uplift of metamorphic rocks in the Alps (France). *Geophysical Journal International*, 108(2), 491–501. <https://doi.org/10.1111/j.1365-246X.1992.tb04630.x>
- Sánchez-Bettucci, L., & Rapalini, A. (2002). Paleomagnetism of the sierra de las animas complex, southern Uruguay: Its implications in the assembly of western Gondwana. *Precambrian Research*, 118(3–4), 243–265. [https://doi.org/10.1016/S0301-9268\(02\)00114-6](https://doi.org/10.1016/S0301-9268(02)00114-6)
- Santana, A., Chemale, F., Scherer, C., Guadagnin, F., Pereira, C., & Santos, J. (2021). Paleogeographic constraints on source area and depositional systems in the Neoproterozoic Itrecê Basin, São Francisco Craton. *Journal of South American Earth Sciences*, 109, 103330. <https://doi.org/10.1016/j.jsames.2021.103330>
- Shi, Q., & Wu, J. (2021). Review on sulfur compounds in petroleum and its products: State-of-the-art and perspectives. *Energy & Fuels*, 35(18), 14445–14461. <https://doi.org/10.1021/acs.energyfuels.1c02229>

- Shulman, G., Yafet, Y., Eisenberger, P., & Blumberg, W. (1976). Observations and interpretation of x-ray absorption edges in iron compounds and proteins. *Proceedings of the National Academy of Sciences of the United States of America*, 73(5), 1384–1388. <https://doi.org/10.1073/pnas.73.5.138>
- Stamatatos, J., Hirt, A., & Lowrie, W. (1996). The age and timing of folding in the central Appalachians from paleomagnetic results. *GSA Bulletin*, 108(7), 815–829. [https://doi.org/10.1130/0016-7606\(1996\)108<0815:taotof>2.3.co;2](https://doi.org/10.1130/0016-7606(1996)108<0815:taotof>2.3.co;2)
- Strehlau, J., Hegner, L., Strauss, B., Feinberg, J., & Penn, R. (2014). Simple and efficient separation of magnetic minerals from speleothems and other carbonates. *Journal of Sedimentary Research*, 84(11), 1096–1106. <https://doi.org/10.2110/jsr.2014.89>
- Szczerba, M., Kłapyta, Z., & Kalinichev, A. (2014). Ethylene glycol intercalation in smectites. Molecular dynamics simulation studies. *Applied Clay Science*, 91–92, 87–97. <https://doi.org/10.1016/j.clay.2014.02.014>
- Tauxe, L., Banerjee, S., Butler, R., & van der Voo, R. (2018). *Essentials of paleomagnetism: Third web edition*. UC Press. Retrieved from <https://earthref.org/MagIC/books/Tauxe/Essentials/>
- Tauxe, L., Mullender, T., & Pick, T. (1996). Potbellies, wasp-waists, and superparamagnetism in magnetic hysteresis. *Journal of Geophysical Research: Solid Earth*, 101(B1), 571–583. <https://doi.org/10.1029/95JB03041>
- Tedeschi, M., Novo, T., Pedrosa-Soares, A., Dussin, I., Tassinari, C., Silva, L. C., et al. (2016). The Ediacaran Rio Doce magmatic arc revisited (Araçuaí-Ribeira orogenic system, SE Brazil). *Journal of South American Earth Sciences*, 68, 167–186. <https://doi.org/10.1016/j.jsames.2015.11.011>
- Temporim, F., Bellon, U., Domeier, M., Trindade, R., Agrella-filho, M., & Tohver, E. (2021). Constraining the Cambrian drift of Gondwana with new paleomagnetic data from post-collisional plutons of the Araçuaí Orogen, SE Brazil. *Precambrian Research*, 359, 106212. <https://doi.org/10.1016/j.precamres.2021.106212>
- Tohver, E., D'Agrella-Filho, M., & Trindade, R. (2006). Paleomagnetic record of Africa and South America for the 1200–500 Ma interval, and evaluation of Rodinia and Gondwana assemblies. *Precambrian Research*, 147(3–4), 193–222. <https://doi.org/10.1016/j.precamres.2006.01.015>
- Tohver, E., Trindade, R., Solum, J., Hall, C., Riccomini, C., & Nogueira, A. (2010). Closing the clymene ocean and bending a brasiliano belt: Evidence for the Cambrian formation of Gondwana, southeast Amazon Craton. *Geology*, 38(3), 267–270. <https://doi.org/10.1130/G30510.1>
- Tohver, E., Weil, A., Solum, J., & Hall, C. (2008). Direct dating of carbonate remagnetization by $^{40}\text{Ar}/^{39}\text{Ar}$ analysis of the smectite–Illite transformation. *Earth and Planetary Science Letters*, 274(3–4), 524–530. <https://doi.org/10.1016/j.epsl.2008.08.002>
- Tolentino, H. (2021). X-Ray microscopy developments at sirius-lns: First commissioning experiments at the carnauba beamline. In *X-ray Nanoimaging: Instruments and methods V* (p. 6). <https://doi.org/10.1117/12.2596496>
- Tolentino, H., Soares, M. M., Perez, C. A., Vicentin, F. C., Abdala, D. B., Galante, D., et al. (2017). CarnaÚba: The coherent x-ray nanoprobe beamline for the Brazilian synchrotron sirius/lns. *Journal of Physics: Conference Series*, 849, 012057. <https://doi.org/10.1088/1742-6596/849/1/012057>
- Torsvik, T., & Cocks, L. (2013). Gondwana from top to base in space and time. *Gondwana Research*, 24(3–4), 999–1030. <https://doi.org/10.1016/j.jgr.2013.06.012>
- Torsvik, T., Van der Voo, R., Preeden, U., Mac Niocaill, C., Steinberger, B., Doubrovine, P. V., et al. (2012). Phanerozoic polar wander, palaeogeography and dynamics. *Earth-Science Reviews*, 114(3–4), 325–368. <https://doi.org/10.1016/j.earscirev.2012.06.007>
- Trindade, R., D'Agrella-Filho, M., Babinski, M., Font, E., & Brito, B. (2004). Paleomagnetism and geochronology of the bebedouro cap carbonate: Evidence for continental-scale Cambrian remagnetization in the São Francisco Craton, Brazil. *Precambrian Research*, 128(1–2), 83–103. <https://doi.org/10.1016/j.precamres.2003.08.010>
- Trindade, R., Font, E., D'Agrella-Filho, M., Nogueira, A., & Riccomini, C. (2003). Low-latitude and multiple geomagnetic reversals in the neoproterozoic Puga cap carbonate, Amazon craton. *Terra Nova*, 15(6), 441–446. <https://doi.org/10.1046/j.1365-3121.2003.00510.x>
- Trindade, R., & Macouin, M. (2007). Palaeolatitude of glacial deposits and palaeogeography of Neoproterozoic ice ages. *Comptes Rendus Geoscience*, 339(3–4), 200–211. <https://doi.org/10.1016/j.crte.2007.02.006>
- Tucker, M. (2001). Sedimentary petrology. In *An introduction to the origin of sedimentary rocks*. Blackwell Science Ltd.
- Wang, Y., Ge, K., Williams, W., Zhou, H., Wang, H., Nagy, L., et al. (2022). Micromagnetic modeling of a magnetically unstable zone and its geological significances. *Journal of Geophysical Research: Solid Earth*, 127(9), 1–14. <https://doi.org/10.1029/2022JB024876>
- Wiedemann, C., Medeiros, S., Ludka, I., Mendes, J., & Costa-de Moura, J. (2002). Architecture of late orogenic plutons in the Araçuaí-Ribeira fold belt, southeast Brazil. *Gondwana Research*, 5(2), 381–399. [https://doi.org/10.1016/S1342-937X\(05\)70730-9](https://doi.org/10.1016/S1342-937X(05)70730-9)
- Woods, S. D., Elmore, R. D., & Engel, M. H. (2002). Paleomagnetic dating of the smectite-to-illite conversion: Testing the hypothesis in Jurassic sedimentary rocks, skye, Scotland. *Journal of Geophysical Research*, 107(B5), EPM2-1–EPM2-10. <https://doi.org/10.1029/2000JB000053>
- Xu, Y., Tan, X., Li, S., Li, Y., Ran, B., Han, Y., et al. (2022). Paleomagnetism of the greater Indian passive margin sediments from the upper cretaceous succession: Evidence for long-delayed remagnetizations and implication for the India-Asia collision. *Journal of Asian Earth Sciences*, 229, 105165. <https://doi.org/10.1016/j.jseas.2022.105165>
- Yamashita, H. (2003). Xafs analysis and applications to carbons and catalysts. In *Carbon Alloys: Novel concepts to develop carbon science and technology* (pp. 189–209). Elsevier Ltd.
- Zhao, H., Cao, Y., Sit, S., Lineberry, Q., & Pan, W. (2012). Thermal characteristics of bitumen pyrolysis. *Journal of Thermal Analysis and Calorimetry*, 107(2), 541–547. <https://doi.org/10.1007/s10973-011-1590-x>
- Zhu, J., Zeng, Z., & Li, W. (2021). K-edge xanes investigation of fe-based oxides by density functional theory calculations. *Journal of Physical Chemistry C*, 125(47), 26229–26239. <https://doi.org/10.1021/acs.jpcc.1c08461>
- Zumaquero, E., Gilabert, J., Díaz-Canales, E., Gazulla, M., & Gómez-Tena, M. (2021). Study on sulfide oxidation in a clay matrix by the hyphenated method. *Minerals*, 11(10), 1121. <https://doi.org/10.3390/min11101121>
- Zunino, F., & Scrivener, K. (2022). Oxidation of pyrite (FES2) and troilite (FES) impurities in kaolinitic clays after calcination. *Materials and Structures*, 55(1), 9. <https://doi.org/10.1617/s11527-021-01858-9>